Unclassified

SECURITY CLASSIFICATION OF THIS PAGE (When Data Entered)

20000828121

AD-A154 163

DTIC FILE COPY

REPORT DOCUMENTATION PAGE

READ INSTRUCTIONS BEFORE COMPLETING FORM

1. REPORT NUMBER: FR-PEC-85	2. GOVT ACCESSION NO. / 3. RECIPIENT'S CATALOG NUMBER: (2)
4. TITLE (and Subtitle): Photoeffects of Semiconductor Electrolyte Interfaces	5. TYPE OF REPORT & PERIOD COVERED: Final Report 1979-1984
	6. PERFORMING ORG. REPORT NUMBER:
7. AUTHOR(s): Terry E. Phillips, K. Moorjani, J. C. Murphy and T. O. Poehler	8. CONTRACT OR GRANT NUMBER(s): N00024-85-C-5301
9. PERFORMING ORGANIZATION NAME AND ADDRESS: Johns Hopkins University Applied Physics Laboratory, Laurel, MD 20707	10. PROGRAM ELEMENT, PROJECT, TASK AREA & WORK UNIT NUMBERS: 61153N RR011-02-03 NR 392-027
11. CONTROLLING OFFICE NAME AND ADDRESS: Office of Naval Research, Arlington, VA 22217	12. REPORT DATE: March 1985
	13. NUMBER OF PAGES:
14. MONITORING AGENCY NAME & ADDRESS (if different from Controlling Office)	15. SECURITY CLASS. (of this report): Unclassified
	15a. DECLASSIFICATION/DOWNGRADING SCHEDULE:

16. DISTRIBUTION STATEMENT (of this Report)

Approved for public release; distribution unlimited

17. DISTRIBUTION STATEMENT (of the abstract entered in Block 20, if different from Report)

18. SUPPLEMENTARY NOTES

(2)

19. KEY WORDS (Continue on reverse side if necessary and identify by block number)

Photoelectrolysis, photoanode, transition metal semiconductor, TiO_2, VO_2, Fe_2O_3, $FeTiO_3$, reduced bandgap, charge transfer absorption, amorphous film, photoconductivity

20. ABSTRACT (Continue on reverse side if necessary and identify by block number)

see attached page

ELECTE MAY 29 1985 A

DD FORM 1 JAN 73 1473 EDITION OF 1 NOV 65 IS OBSOLETE

S/N 0102-LF-014-6601

Unclassified

SECURITY CLASSIFICATION OF THIS PAGE (When Data Entered)

85 4 22 105

Photoeffects at Semiconductor Electrolyte Interfaces

T. E. Phillips, K. Moorjani, J. C. Murphy, and T. O. Poehler

The Johns Hopkins University, Applied Physics Laboratory
Johns Hopkins Road
Laurel, MD 20707

FINAL REPORT

March 1985

Report Number FR-PEC-85

Abstract

Materials based on modified transition metal oxide semiconductors for the photoelectrochemical decomposition of H_2O were investigated. Single crystals of TiO_2 doped with VO_2 were made and it was demonstrated that the bandgap was decreased from 3.03 eV to 1.99 eV. The flatband potential was increased from -1.0 V to 0.25 V. Both effects are attributed to the existence of an empty vanadium d-band located in the TiO_2 bandgap. Another approach was taken with $FeTiO_3$-Fe_2O_3 alloys in the form of amorphous thin films and single crystals, where it was anticipated that the charge-transfer interactions observed in such alloys could be exploited in the materials' photoelectrochemical properties. The effect of $FeTiO_3$ had very little effect on the overall properties of Fe_2O_3 single crystals. On the other hand the effect on the Fe/Ti oxide thin films was quite dramatic. Optical absorption, photoconductivity and photoelectrolytic spectral measurements demonstrate a photometric enhancement at energies above the bandgap for Ti concentrations in the range of 5% to 8%. There is some suggestion that the bandgap has been reduced in this concentration regime. Higher concentrations of Ti result in a change from n-type to p-type. Efficiency and stability of thermally oxidized Fe/Ti oxide films are comparable to single crystal results.

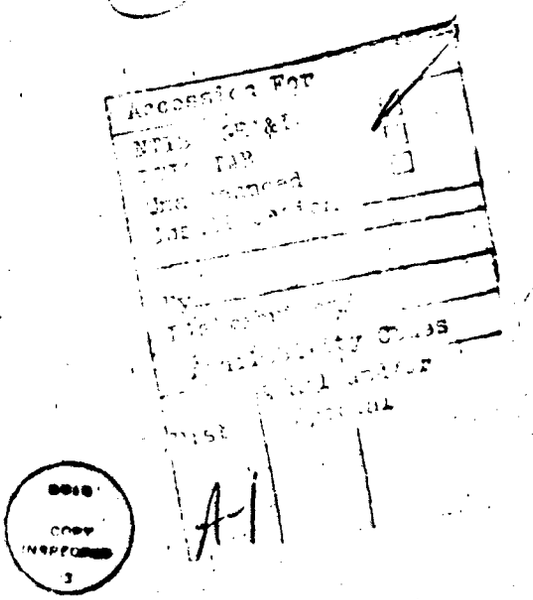

Table of Contents

TiO_2-VO_2 Alloys -- Reduced Bandgap Effects in the Photoelectrolysis of Water

T. E. Phillips, K. Moorjani, J. C. Murphy, and T. O. Poehler
Johns Hopkins University, Applied Physics Laboratory
Johns Hopkins Road
Laurel, MD 20707

ABSTRACT

A series of $Ti_{1-x}V_xO_2$ ($0.04 \leq x \leq 0.55$) single crystals and ceramics were prepared and evaluated as electrodes in the photo-assisted electrolysis of H_2O. Samples of $Ti_{1-x}V_xO_2$ ($0.3 \lesssim x \lesssim 0.5$) possess an optical bandgap of 1.99 eV and a flatband potential of approximately +0.05 $V_{vs.SCE}$, which compares with 3.03 eV and -1.0 $V_{vs.SCE}$ respectively in TiO_2. For $Ti_{1-x}V_xO_2$ in the range $0.10 \lesssim x \lesssim 0.30$, the flatband potential increases to approximately 0.25 $V_{vs.SCE}$. Both observations, the narrower bandgap and varying flatband potential, are attributed to the existence of a primarily V d-band, of varying width and density, interjected in the TiO_2 bandgap.

Full paper was published in the Journal of the Electrochemical Society, Vol. 129, p. 1210 (1982).

Photoelectrochemistry of Iron-Titanium Oxide Alloys

T. E. Phillips, K. Moorjani, J. C. Murphy, and T. O. Poehler

Johns Hopkins University, Applied Physics Laboratory

Laurel, MD 20707

The following section is to be submitted for publication

in the Journal of the Electrochemical Society

INTRODUCTION

The observation of photo-assisted decomposition of water into elemental constitutents by the action of light on a semiconductor-electrolyte interface is now a well-documented phenomenon. The first observation of this effect was made in 1972 by Fujishima and Honda,[1] and since then, research in this area has been quite intense, to exploit its obvious solar energy conversion potential.[2,3] Although much effort has been expended, a practical solar energy conversion scheme remains elusive due to challenging materials problems.

There are a number of criteria that must be met by a material if it is to be considered a potential candidate for solar-powered photoelectrolysis of water; three of these are considered to be of primary importance. The first criterion is that of a suitable bandgap for the material. Much of the solar photon flux lies in the 1.4-2.0 eV range and to achieve high conversion efficiencies, the material must have, among other conversion efficiency related properties, a bandgap that lies in this range. Secondly, the material must be chemically stable. The photoelectrolytic process that occurs at the semiconductor-electrolyte interface relies, in most part, on the production of energetic species (minority carriers) within the semiconductor, and the semiconductor must be able to withstand their presence. To date, most of these materials which are chemically stable, also have bandgaps outside the prerequisite 1.4 to 2.0 eV range. The transition metal oxides are good examples of this problem. They are typically very stable in most electrolytes, but their bandgaps range from 2.8 to 3.8 eV.

There are a few materials that do possess both the required bandgap and chemical stability, but they do not satisfy the third requirement regarding the proper positioning of the valence and conduction bands relative to the

redox levels of the solution. For example, with an n-type semiconductor, it is necessary that the conduction band be at the same position or lie higher than the H^+/H_2 redox potential in order to achieve photoelectrolysis without the application of an external bias.

Our work has concentrated on starting with materials which are intrinsically stable under photoelectrolytic conditions and can be modified to improve their correspondence with the solar spectrum and their electrochemical efficiency.[4]

BACKGROUND AND FOCUS

Currently, our attention has been focused on a variation of the transition metal oxide, Fe_2O_3. In the past, n-type Fe_2O_3 has been demonstrated to possess very good stability against photoanodic decomposition in non-acidic (pH > 6) environments. Its bandgap of 2.0-2.2 eV is one of the smallest of the transition metal oxides and is quite close to being ideal for the efficient utilization of the solar flux profile in photoelectrolytic applications.

With respect to the negative aspects of this material, there are a few, but we believe that they are correctable. One such disadvantage is that the flatband potential (V_{FB}) is not sufficiently negative to effect the unassisted photoelectrolysis of water, though a tandem p-n cell would be more than capable of unassisted photoelectrolysis. Another problem area is that of efficiency. There appears to be some consensus in the literature that the quantum effficiency and therefore the photoelectric conversion efficiency of n-type Fe_2O_3 is low in comparison to other transition metal oxides. Interestingly though in our work and in some other reports, the efficiency is

found to be very respectable. The reason, we believe, for the inconsistency in the various reports is a result of the material's (n-type Fe_2O_3) sensitivity to preparation.

It has been demonstrated[5] that pure α-Fe_2O_3 is photoelectrochemically inactive. Activation of α-Fe_2O_3 appears to require the presence of Fe^{+2}, usually in the form of Fe_3O_4. The difficulty of obtaining reproducible results from Fe_2O_3 probably arises from the difficulty of controlling the amount and homogeneity of the structurally incompatible (spinel) Fe_3O_4 in the bulk (corundum) Fe_2O_3. In most preparations of the n-type Fe_2O_3, the Fe_3O_4 is presumably found on or near the surface and along dislocation networks (forming at grain boundaries) where the spinel structure is more easily accommodated. Consequently, the observed photoconductive and photoelectrochemical properties can be significantly affected by the preparation techniques, which may overshadow the intrinsic properties of Fe_2O_3. With these problems in mind, we are looking at a charge-transfer alloy of Fe_2O_3 and $FeTiO_3$ as an interesting candidate for use as a photoelectrode.

α-iron oxide and iron titanate crystallize in essentially the same rhombohedral space group ($R\bar{3}C/R\bar{3}$) with similar lattice constants. Consequently Fe_2O_3 and $FeTiO_3$ form a solid solution over the whole composition range.[6] As a naturally occurring mineral, the hematite (iron oxide)-ilmenite (iron titanate) series are very important in paleomagnetic research because they exhibit highly stable magnetic properties which are dependent on composition and thermal history.[7] In many minerals, the electrical and optical properties that characterize these materials are principally determined by intervalence charge transfer and crystal field transitions within and between cations of Fe and Ti.

In the hematite-ilmenite mineral series [$xFeTiO_3 \cdot (1-x)Fe_2O_3$], Mossbauer measurements[6] indicate that for $x \leq 0.6$, there is a considerable amount of charge transfer from Fe^{+2} in the titanate to Fe^{+3} in the hematite. For many minerals where the crystal field interactions of the participating ions are different, the energy of this charge transfer reaction is often found in the visible region of the spectrum. We were interested in examining the effects of these interactions ($Fe^{+2} \rightarrow Fe^{+3}$; $Fe^{+2} \rightarrow Ti^{+4}$; and $Ti^{+3} \rightarrow Ti^{+4}$) when introduced into the Fe_2O_3 photoelectrochemical system.

Our specific area of interest was in changes of the spectral response of the modified Fe_2O_3 as a consequence of the additional absorption sites, $Fe^{+2} \rightarrow Fe^{+3}$; $Fe^{+2} \rightarrow Ti^{+4}$; and $Ti^{+3} \rightarrow Ti^{+4}$. Additionally, we wanted to evaluate the stabilization of the semiconducting properties by the introduction of Fe^{+2} ions contained within a nearly identical crystal lattice, as opposed to the introduction via a structurally incompatible Fe_3O_4 spinel structure. Finally, we investigated changes in the other photoelectrochemical parameters of interest such as quantum efficiency and flatband potential in this alloy system.

A series of $Fe_{1-x}Ti_xO_y$ samples were prepared in the form of thin films by r.f. reactive sputtering and thermal oxidation techniques, and single crystals by flux melt techniques. The thin films are believed to be $(\frac{x}{2})FeTiO_3 \cdot (1 - \frac{x}{2})Fe_2O_3$, based on assumptions derived from X-ray measurements, and the single crystals are known to be $FeTiO_3/Fe_2O_3$. With respect to the thin films, their optical, photoconductivity, and photoelectrochemical behavior were examined as a function of Ti concentration, and these results are presented in the following section. The single crystals were evaluated for changes in their photoelectrochemical properties as a function of $FeTiO_3$

concentration and the results are presented in the section following the thin film work.

THIN FILMS

Preparation

Thin films of $Fe_{1-x}Ti_xO_y$, used for absorbance and photoconductivity measurements, were prepared on one inch square glass slides (Corning #7024) by r.f. reactive sputtering Fe-Ti metal powder mixtures. The gas used to generate the sputtering plasma was a mixture of Ar (5 microns Hg) and O_2 (5 microns Hg). Deposition time was typically three hours with a 450 watt r.f. source (13.58 MHz).

Thin films used in the photoelectrolysis measurements were prepared by two different techniques. The first series, hereafter known as r.f. oxides, were made in a manner similar to that described above, except that a thin metal layer is first deposited on the glass slide. This metal layer, which is used as an electrical contact to the subsequently deposited metal oxide layer, is produced by sputtering the Fe-Ti powder target with 5 microns of Ar for 1.5-6.0 hours in the absence of O_2. Longer deposition times were required as the per cent of Ti increased. The r.f. sputtered metal oxide film is then applied to the Fe-Ti metal contact through a 3/4" circular mask. The starting compositions of the Fe-Ti metal powder mixtures were 0.0, 7.7, 22.6, 26.2, 31.8, 43.7, 53.8, and 74.5 (per cent titanium by moles).

The second series of thin films, referred to as the thermal oxides, were prepared by sputtering the Fe-Ti metal powder mixtures onto one inch square glass slides for varying times (0.5-9.0 hours), with 5 microns of Ar in the

absence of O_2. The resulting thin metal films were then oxidized by placing them on a 300°C hot plate under the ambient atmosphere for 0.5 to 2.0 hours. The starting compositions of the Fe-Ti metal powder mixtures were 0.0, 7.7, 15.2, 22.6, 31.8, and 53.8 (per cent titanium by moles).

Elemental and Structural Analysis

The initial composition of the Fe-Ti metal powders used as the sputtering target for the various films produced was well-known. Since the sputtering rates of Fe and Ti differ, and appear to be sensitive to the sputtering conditions, such as the O_2 and Ar partial pressure, the final thin film composition may be considerably different from the initial composition.

Elemental analyses were performed by sputter ion mass spectroscopy. Matrix yield factors were obtained from powders of Fe_2O_3, Fe_2TiO_5, and Fe_2TiO_3. When a composition is reported in brackets [x], it implies that the composition was not determined explicitly for that particular sample, rather it was obtained from a film produced from the same Fe/Ti powder target. Table 1 lists the starting and final composition of some of r.f. and thermal oxides examined.

Table 1. Elemental analysis of thin film oxides as determined by SIMS.

Starting Composition %Ti	r.f.oxides %Ti	Thermal Oxides %Ti
0	0	0
7.7	1.2	
15.4	2.5	2.5
22.5	4.4	4.5
26.2	3.3	4.2
31.8	5.3	6.4
43.7	7.2	
53.8	11.4	16.5
74.5	16.9	

Normally energy dispersive spectroscopy is the preferred technique for obtaining stoichiometry because of the greater simplicity and ease of measurement. In the case of the thin films though, the Ti determination was seriously hampered by a Ba impurity in the glass substrate.

X-ray diffraction measurements were made on the r.f. oxide films (with and without the underlying metal layer) and on the thermal oxide films with a Reed camera using Cr K_α radiation. Diffraction measurements were made on the bare metal film, on the oxide film plus underlying metal film and in the case of the transparent r.f. oxide films without an underlying metal layer, on just the oxide film. The X-ray beam was incident on the front surface of the films at an angle of 75° from the normal and the recorded diffracted rays similarly emanated from the front surface. The thickness of the oxide layers are estimated to be 600A-1300A and the unoxidized metal films are 1000A-1800A.

The pure iron films were identified to be of the α-Fe structure without orientational dependence. The angular width of the diffraction lines visually estimated at half maximum was 1.2°(2θ=69°). This is considerably larger than the 0.2° line widths observed in a polycrystalline film of comparable thickness which is a reasonable upper limit due to instrumental broadening factors. The addition of Ti causes the diffraction linewidth to increase and the higher 2θ lines 200 and 211 to decrease in intensity. At 4.5% Ti just one line corresponding to the 110 reflection of α-Fe remained. This behavior persists up to approximately 11% Ti, where the linewidth of the single diffraction line is 1.6°. At a higher Ti concentration, ~ 16%, the single line is replaced by two very weak and broad lines tentatively assigned to the intermetallic TiFe.

In some of the films examined, the presence of FeO was observed, which is normally produced only at high temperatures (> 570°C) under equilibrium conditions. It is felt that the FeO is most likely formed at the glass/metal

interface during the initial stages of the metal film deposition, where the kinetically "hot" Fe atoms can react with oxygen, adsorbed or otherwise, available at the surface.

The oxide films with an underlying metal film, including both the r.f. oxide and the thermal oxide films, yielded results identical to that of the bare metal films. As the additional oxide layer did not result in any observable coherent diffraction, the oxide layers are assumed to be amorphous in structure. The r.f. oxides without an underlying metal film were likewise void of any obvious diffraction lines. Through the use of some photographic enhancement techniques, a very weak diffraction pattern of 6-10 lines could be observed in some of the films. The pattern is consistent with the $Fe_2O_3/FeTiO_3$ corundum structure, $R\bar{3}C/R3$.

Attempts to produce a thin film of an amorphous Fe/Ti oxide without the underlying metal layer, by the technique used to make the thermal oxides, were unsuccessful. The nominally amorphous oxide films growing from the underlying metal film would crystallize when all or most of the metal was consumed, and the resulting oxide films adhered poorly to the glass substrate. The polycrystalline nature of these films was indicated by their strong X-ray diffraction pattern which was unambiguously assigned to the $Fe_2O_3/FeTiO_3$ structure.

Although the composition in the amorphous oxide films has not been explicitly determined, it is felt that the composition and short-range order are very likely that of $Fe_2O_3/FeTiO_3$. Consequently the results presented in the succeeding sections will occasionally be discussed in terms of the properties of Fe_2O_3 and $FeTiO_3$.

Experimental Procedure

Absorptivity Measurements

Absorbance measurements were made with a Beckman DK-2 from 400 nm to 1800 nm. The short wavelength limit was set by the non-linearity of the detector at the high absorbance (>1.5 A) values of the films. All of the oxide films exhibited normal reflectance losses and most of the films were of a thickness that interference effects were obvious in the 700 nm to 400 nm region. These interference effects extended to the 1800 nm limit, where it was assumed that the oxide films did not exhibit any inherently measureable absorbance. Using derived film thickness values from the SIMS data, an iterative process was used to calculate a best fit index of refraction (n) and thickness (d) for each film. The best fit was determined by a non-linear squares minimization of deviations in the absorbance data from the baseline in the 800 nm to 1800 nm region. The values of n and d were then used to correct the measured absorbance for reflectance effects and thickness in the 400 nm and 700 nm region. No attempt was made to account for the anomolous dispersion of n within the absorption band. The value of n varied from 2.46 to 2.71. The optimum d was typically 6%-10% larger than the d determined from the SIM data.

Photoconductivity

The photoconductivity of the samples used for the absorbance measurements was measured by making electrical contact to the sample with silver paint to two points separated by 1 cm, along the edge of the film. A 50 volt potential was applied to one contact and the other contact was terminated at the

inverting-input of a high input-impedance operational amplifier (RCA CA3140). The amplifier was operated with a gain of 10^8 V/A and a low-pass cutoff of 30 Hz. (-3.0 db.).

Monochromatic light was obtained from a Spex Minimate Monochromator with a 100 W quartz-halogen source. A 20 nm bandpass was achieved with 5 mm slits. The light was chopped at 23 Hz by a mechanical chopper. The wavelength dependence of the photocurrent was then corrected for the source and monochromator profile, which was measured with a Laser Precision Corp. Power Meter Rk 3240. Typical light intensities ranged from 0.03 mW/cm^2 at 400 nm to 0.2 mW/cm^2 at 570 nm.

Photoelectrolysis

Thin film samples that were used for photoelectrolysis measurements were prepared by breaking the one inch square glass slides containing the metal oxide thin film into two to four pieces. A copper wire was bonded to the underlying metal layer with silver paint. The front and side surface of the sample was then encapsulated in Torrseal epoxy except for a small circular area (3-5 mm diameter) on the surface. All of the samples were illuminated through a 5 mm^2 mask placed near the front surface of the electrode.

The photoelectrochemical (PEC) cell is a conventional three-electrode cell with a 1 cm^2 platinum counter electrode and a saturated calomel (SCE) reference electrode. The electrolyte used in all measurements was 1.0 M NaOH. All solutions were de-aerated by bubbling N_2 through the solution. The three-electrode potentiostatic measurements were made with a PAR 173 Potentiostat linked with a lock-in amplifier to determine light induced changes in cell current. A description of the light source can be found in the photoconductivity section.

Differential Capacitance

The capacitance of a semiconductor-electrolyte interface is determined by several interfacial processes and in general depends on the interfacial voltage. One important component of the overall capacitance is the capacitance of the space charge region. This space charge capacitance is a function of the width of the depletion region which in turn is dependent on the voltage$^{1/2}$ impressed across the semiconductor. Given that other complicating contributions to the overall capacitance such as traps, surface states, and the Helmholtz capacitance are well-behaved or can be predicted, the linear relationship of (space charge capacitance)$^{-2}$ to the interfacial voltage can be used to characterize the semiconductor's flatband potential and charged impurity density.

We have measured the differential capacitance of the r.f. and thermal oxides using the same experimental configuration as used for the photoelectrolysis measurements, except that the sample was held in the dark. A linear voltage ramp with a superimposed 2.0 mV sinusoidal a.c. voltage was applied to the sample. Three frequencies were used, 23, 500, and 100 Hz. The limits of the ramp were typically -1.0 V to +0.8 V (versus SCE), with ramp speeds of 5-10 mV/second. The normal (i_0) and quadrature (i_{90}) a.c. currents were detected by two HR-8 lock-in amplifiers, and were used to calculate the capacitance as a function of applied voltage using a series resistor-capacitor combination as a model for the system.

In most of the films substantial dark current was observed at the two extremes of the cathodic and anodic potential sweeps. This current is presumably due to faradaic processes at the interface involving the semiconductor or possibly just the underlying metal via pinholes through the oxide. The

presence of this d.c. dark current indicates that the measured i_0 exceeds the actual a.c. current as a consequence of this d.c. current path. This in turn detrimentally affects the determination of the space charge capacitance from a series RC network model. In order to account for this d.c. path, a resistor was added to the model across the space charge capacitance. Inversion of the resulting equations to yield the values of the three component impedences as a function of i_0, i_{90} and $i_{d.c.}$ was straightforward, but applying them to the data was unsuccessful. The problem appears to be the presence of galvanic potentials within the interface which cause the faradaic resistance to be incorrectly determined. This then causes the i_0 to be incorrectly calculated, sometimes leading to negative impedences.

In retrospect it is evident that in order to properly model the interface with enough elements to account for all the ongoing processes and to determine the value of those elements, numerous measurements at different frequencies must be made. As it is not possible to analytically invert the resulting equations to yield the circuit parameters from $i_0(f)$ and $i_{90}(f)$, some sort of least-squares algorithm must then be utilized.

Results

Absorptivity

The absorptivity spectra of the r.f. oxides without an underlying metal layer are presented in Figure 1. Taking the 0% curve as a point of reference, the addition of 4.4% to 5.3% Ti causes the absorptivity to increase in the 500-600 nm region. As the Ti concentration increases beyond 5.3%, the absorptivity begins to drop as the curve appears to be blue-shifted. This would be

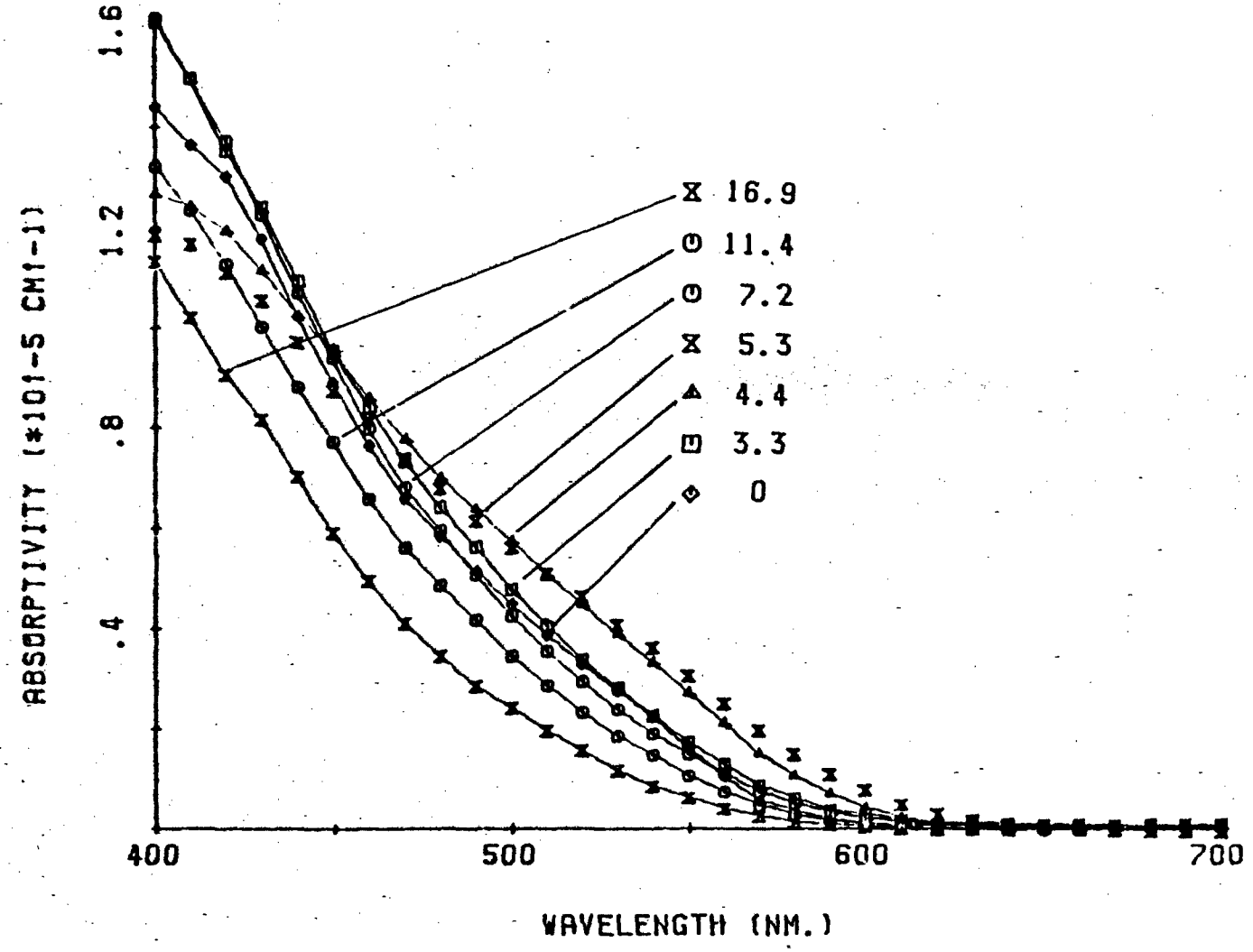
ABSORPTIVITY (*10!-5 CM!-1)
1.6
1.2
.8
.4
400
500
600
700
WAVELENGTH (NM.)
16.9
11.4
7.2
5.3
4.4
3.3
0

FIGURE 1

expected if it is assumed that the increasing Ti concentration is in the form of $FeTiO_3$, which has an E_{gap} of 2.58 eV.[8] The film's spectral response should then at some point reflect the fact that the $FeTiO_3$ content is increasing.

In semiconductors, the optical absorption coefficient near the edge is given by the equation;[9]

$$\alpha_{h\nu} = A(h\nu - E_{gap})^{n}/h\nu$$

where the exponent n is determined by the nature of the transition. For a direct transition, n = 1/2; forbidden direct, n = 3/2; and indirect, n = 2. When the data in Figure 1 are plotted in the form $(\alpha h\nu)^{1/2}$ vs. hν, the linear relationship that is seen indicates that the bandgap transitions are indirect.

The energy range over which the linearity exists varies somewhat with the Ti concentration. From 0% to 5.3% the plots are linear from just above the abscissa intercept to approximately 2.3 eV. At 2.3 eV, the slope decreases by a small but noticeable amount and the curve is again linear to 3.1 eV, the upper limit of the measurement. In films with Ti concentration above 5.3% and up to 16.9%, the plots are linear from the abscissa intercept to 3.1 eV.

The semiconductor's bandgap can also be determined from the abscissa intercept of the above plots. The values for the bandgap as a function of Ti are given in Table 2, where it is seen that the values drop from 2.08 eV to 1.88 eV in the range of 0% to 5.3% Ti. Beyond 5.3% Ti, the bandgap increases and quickly reaches a value of 2.0 eV. Note that the bandgap of 2.0 eV observed for the film containing 16.9% Ti is lower than one might have expected given the spectrum shown in Figure 1.

With the present films, the bandgap determination is made less certain by some curvature in the immediate vicinity of the intercept; the curvature being more noticeable in the lower Ti content films. This behavior can result from band tailing, and given the highly disordered and/or amorphous nature of these oxide films, it is not at all unexpected.

Table II

Bandgap as a function of Ti concentration, determined from the absorptivity data.

%Ti	Bandgap (eV)
0	2.08
3.3	2.0
4.4	1.94
5.3	1.88
7.2	1.98
11.4	2.0
16.9	2.0

Photoconductivity

All of the spectra were normalized to 400 nm to minimize skewing of the data presentation by such scaling effects as uncertainties in electrode placement, and excitation beam placement and uniformity. The photoconductivity spectrum reflects not only the absorption characteristics of the

material, but also the electrical conductivity characteristics of the film as well. The relationship between the photoconductivity spectrum taken under steady state conditions and the absorption spectrum is given for a single carrier type by the equation:[10]

$$\frac{i(\lambda)}{V} = e\mu\tau n I_0(1-R)(1-\exp(-\alpha(\lambda)d))$$

where μ is the carrier mobility, τ is the carrier recombination lifetime, n is the quantum efficiency of carrier formation, R is the reflectance, α is the absorptivity, and d is the film thickness. In thin films, the reflectance and transmittance ($\exp(-\alpha(\lambda)d)$) terms must be adjusted for multiple reflection effects. The data presented in Figure 2 for the r.f. oxides have been corrected for interference effects and also have been adjusted for a film thickness of 760Å, the average thickness of the films examined. Corrections were also made for the source profile and monochromator response.

It should be recognized that although it is necessary to account for the multiple reflections in the thin film in order to determine the photoconductivity spectrum, the procedure is subject to considerable error. Probably the most serious source of error, in the present case, is the assumption that the product term $n\mu\tau$ is uniform throughout the film. It is certainly reasonable to expect that $n\mu\tau$ near the two film interfaces is going to be different than what it is in the film bulk, but there is no straightforward way to determine this distribution.

As can be seen in Figure 1 and 2, the photometric responses are similar in that a distinct redshift is observed with increasing Ti content followed by a reversal of that trend beyond some Ti concentration. The turnaround in the

Normalized photoconductivity as a function of wavelength for the r.f. oxide series of Fe/Ti oxide thin films. Values were normalized to the value at 400 nm, and calculated for a film thickness of 760 A.

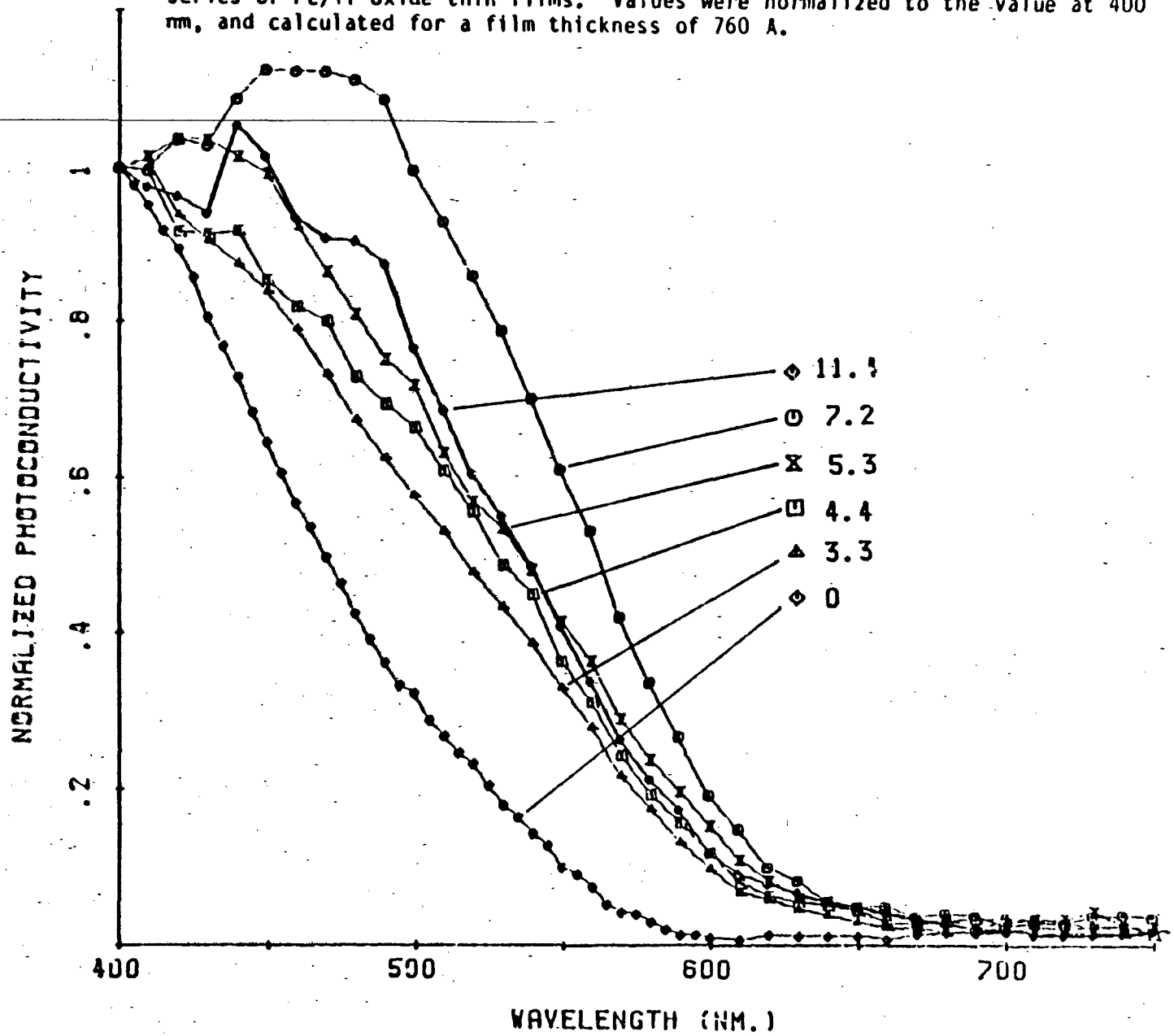

FIGURE 2

photoconductivity occurs around 7.2% Ti in comparison to the 5.3% Ti seen in the absorptivity data. Unfortunately there is only one photoconductivity curve (11.4%) which defines this reversal. The photoconductivity data from the higher Ti content film, 16.9%, was very noisy, and a well defined value at 400 nm could not be determined.

Photoelectrolysis

The photocurrent response as a function of applied voltage was measured for both the r.f. oxide and thermal oxide films. The wavelength chosen was in the range from 450 nm to 470 nm, which represented the maximum in the data before it is corrected for the source and monochromator response.

The films demonstrated an interesting and unusual dependence on the applied voltage. R.f. oxide and thermal oxide films containing lower concentrations of Ti (< 5.3%) exhibited two maxima in their photoanodic current response vs applied voltage. R.f. oxide films containing the higher concentrations of Ti possessed both a photoanodic and a photocathodic current response depending upon the applied potential.

An example typical of the lower Ti content films is shown in Figure 3, which shows the photocurrent verses applied voltage of a [4.4%] Ti sample at 450 nm. As the voltage is swept anodically, the photocurrent begins to rise at -0.75 V (onset potential). It reaches a maximum at -0.33 V, drops through a minimum at -0.05 V and then begins to rise again, peaking usually at +0.45 V. These values are shifted positively for the [5.3%] Ti samples. The onset potential (V_{on}), first peak and valley, are typically -0.50, -0.15, and +0.05V, respectively. Beyond [5.3%], V_{on} and the first peak appear to shift back slightly to more cathodic potentials. Some of the uncertainty in

Photocurrent as a function of applied voltage for a [4.4%] Ti c.f. oxide sample, λ = 450 nm; intensity = 1.8 mW/cm^2; sample area = 5 mm^2.

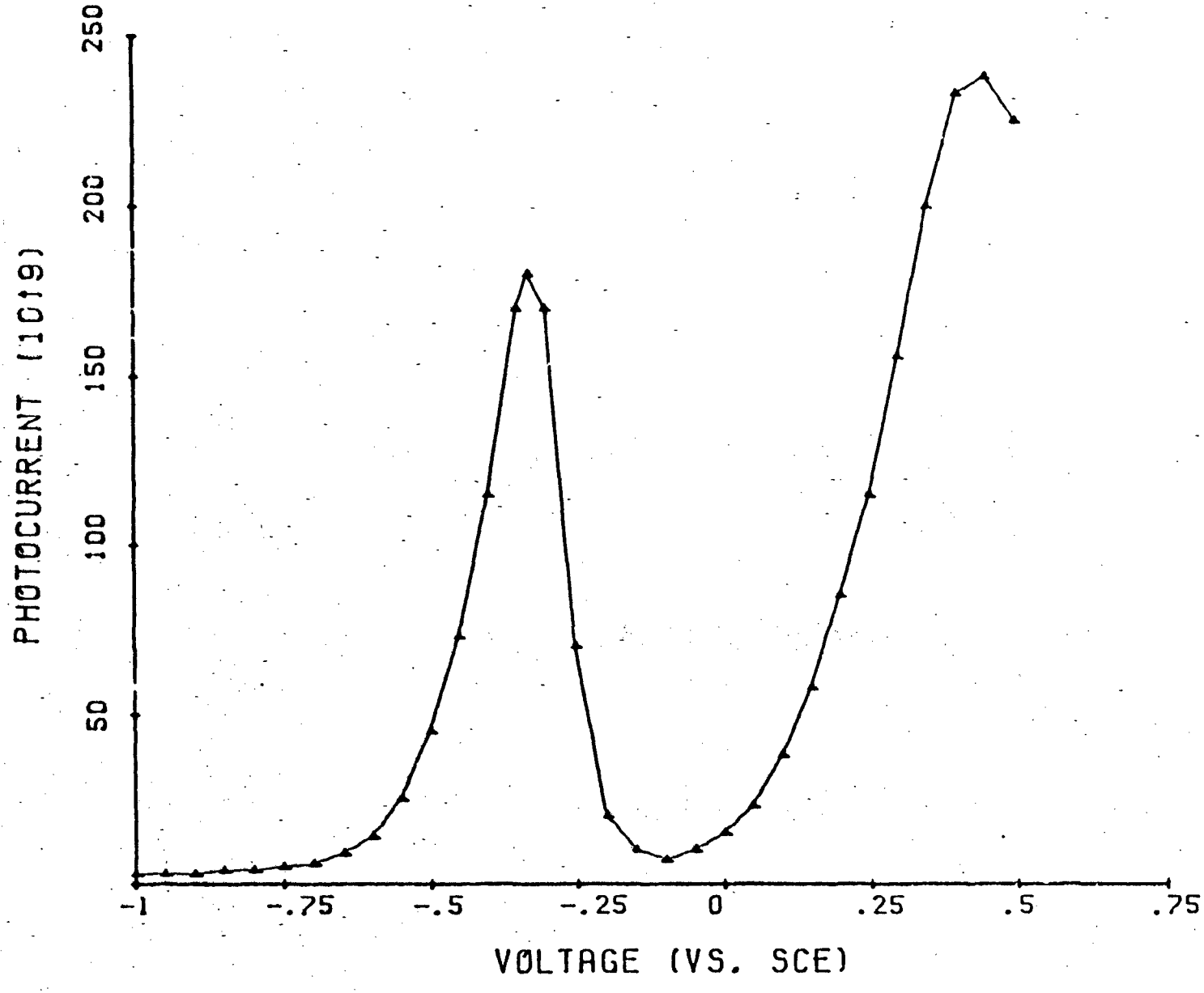

FIGURE 3

determining the precise behavior is a consequence of the photocathodic current (see below) which is becoming more pronounced in this concentration regime. The relative magnitudes of the two peaks varied from sample to sample, with the second peak at +0.45 V usually greater than the first peak, though in many samples the peak heights were equal. R.f. oxides containing 0% Ti did not show a peak at -0.40 to -0.15 volts and the onset potential was typically -0.5 V. The magnitude of the photocurrent maxima (@ 0.45 V; 450 nm - 470 nm) were within a factor of three for most of the films. At the lower Ti concentrations (<7.2%) there was more variation observed in the maxima between different samples of the same composition than between the average value of the maxima at different compositions. There may have been some decrease in the magnitude of the maximum for the higher Ti content samples, but the variation from sample to sample makes it difficult to say with certainty.

The photocurrent versus applied voltage behavior described above was typical of all the samples with a Ti content <[5.3%] after they had been cycled cathodically at least once. Many samples, when scanned cathodically for the first time, exhibited what might be called p-type behavior, i.e., an increasing photocathodic current, as the potential is scanned cathodically. If the potential is allowed to exceed ~-0.7 V, this p-type behavior is replaced by the usual n-type response (the peak at -0.40 to -0.15 V), when the sample is returned to more positive potentials.

The photocurrent versus applied potential response (@ 450 nm - 470 nm) of samples with Ti concentration >[5.3%] showed an increasing predominance of this p-type photoresponse. Unlike the [5.3%] Ti and lower samples, the p-type response tended to be stable as well as more dominant in the higher Ti concentration samples. Figure 4 depicts the photoresponse of a [16.9%] Ti sample,

Photocurrent as a function of applied voltage for a [16.9%] Ti_2 r.f. oxide sample, λ = 450 nm; intensity = 1.8 mW/cm^2; sample area = 5 mm^2.

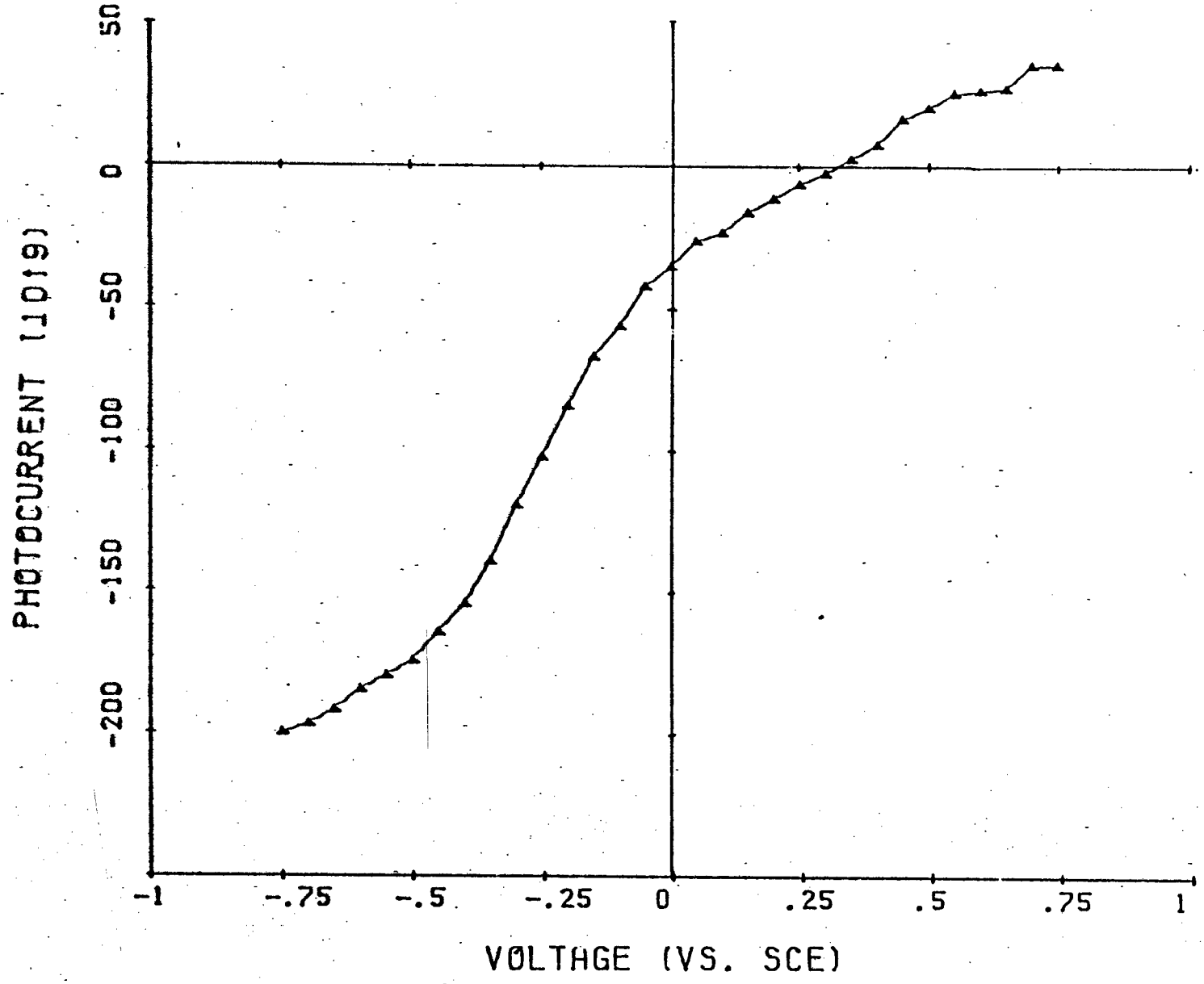

FIGURE 4

in which the p-type photocurrents are evident at potentials less than +0.2 V. This p-type photocurrent was stable and reproducible even after a number of negative (~-0.75 V) voltage excursions.

The photocurrent versus applied potential characteristics of the thermal oxides differs somewhat from the r.f. oxides. The curves observed with the thermal oxides were very similar to the curve seen with the lower Ti content r.f. oxides (Figure 3) with some exceptions. For the lower Ti content thermal oxides, including the 0% sample, a small peak was seen at -0.55 V to -0.50 V, when the sample was scanned anodically from -0.75 V. The onset potential was approximately -0.75 V. A second and much larger peak occurred at +0.55 V, coincident with the rise in the d.c. dark current. At higher %Ti compositions the peak was replaced by a low level plateau in the region from -0.55 to 0.0 V. At no time did any of the thermal oxide films show any evidence of the photocathodic currents that were observed in the higher Ti content r.f. oxide samples.

The magnitude of the photocurrent at the 0.5 V peak does not appear to be a measurable function of the Ti content. There was in fact very little variation observed sample to sample. Relative to the r.f. oxides, the magnitude of the thermal oxide 0.5 V peak was typically 5-10 times larger.

Photocurrent measurements as a function of wavelength were also made on the r.f. oxide and thermal oxide films. Figure 5 depicts the photocurrent spectrum for the series of r.f. oxides at an applied potential of 0.0 V (vs SCE). As was done with the photoconductivity curves, these curves were also corrected for the source and monochromator profile, and all the curves were normalized so that the photocurrents at 400 nm were equivalent. Corrections for multiple internal reflections within the thin films were not attempted,

Relative photocurrent as a function of the excitation wavelength for the r.f. oxide series of Fe/Ti oxide thin films. Each curve is normalized to 400 nm and has been corrected for variations in the excitation intensity. The solution is 1 M NaOH. The applied potential to each sample was 0.0 V (vs SCE).

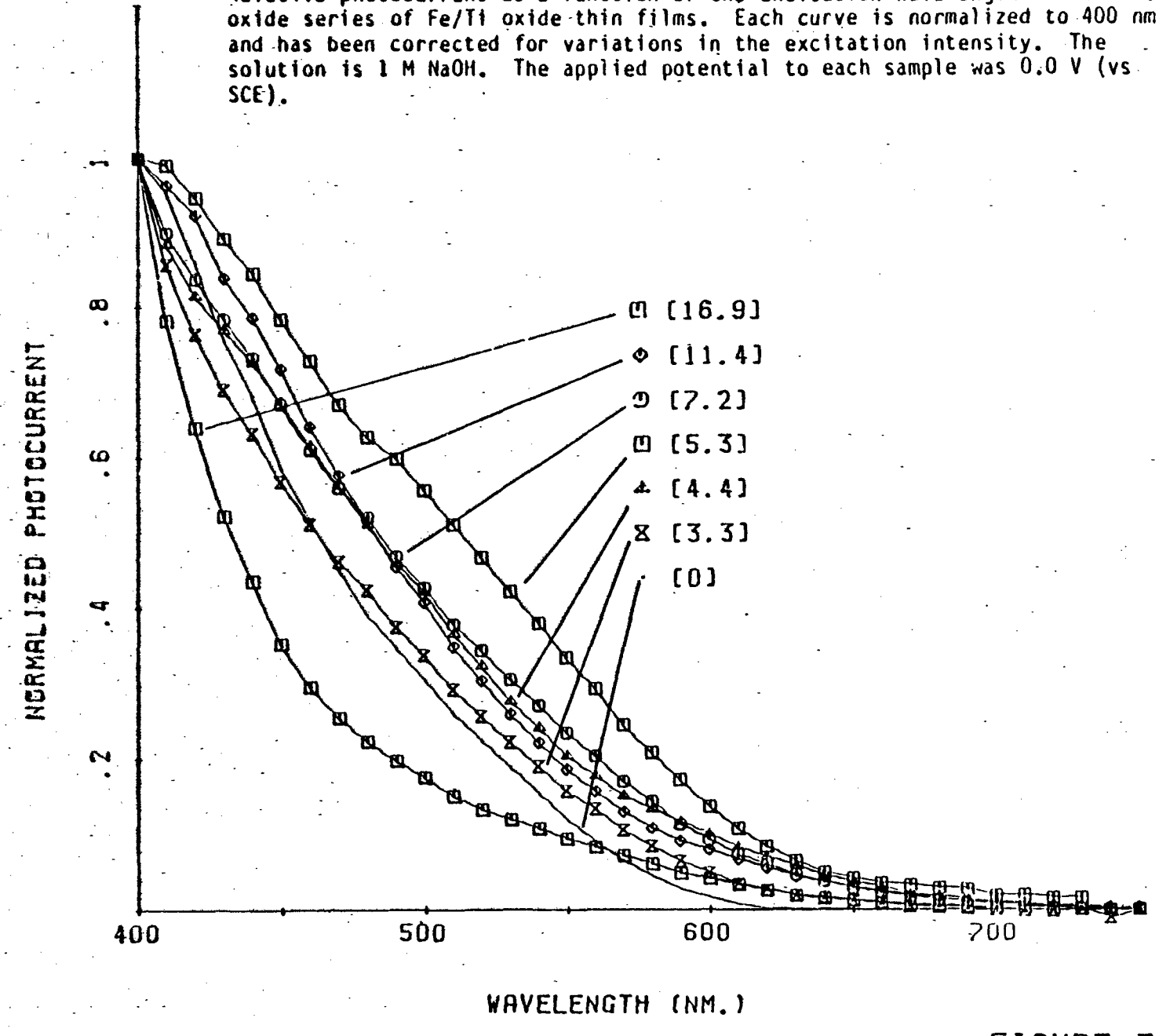

FIGURE 5

however, because of uncertainties in the width of the space charge region and to a lesser degree, in the width of the oxide film.

Taking the 0.0% curve as a point of reference, the relative photoresponse in the 450-600 nm region is enhanced for the lower Ti content samples [4.4%-7.2%]. As the concentration increases above 7.2%, the response in this wavelength region begins to fall back to the 0% reference curve, a characteristic which was similarly observed in the absorptivity and photoconductivity. Note also that the addition of Ti extends the photoresponse of these oxides beyond the 620 nm (2.0 eV) bandedge of Fe_2O_3. All of these curves, except the [16.9%] represent anodic photocurrents from an n-type semiconductor. The [16.9%] curve on the other hand represents a cathodic photocurrent, that one would expect from a p-type semiconductor.

Near the bandedge, where the product of the absorption coefficient (α) and depletion layer width (W) is less than 1 ($\alpha W << 1$), it can be assumed that the photocurrent is proportional to the absorption coefficient. With this relationship, the transition type and bandgap can in principle be calculated in a manner identical to that done with the absorptivity data. And as was observed with the absorptivity data, the transition type is most likely indirect. The bandgap determination is less certain though, because the curves exhibited much more curvature than seen in the $(\alpha \cdot h\nu)^{1/2}$ vs $h\nu$ plots of the absorptivity data. The 0% Ti curve was the only one which was reasonably linear and the intercept at 2.0 eV is consistent with the absorptivity data. An increase in Ti was accompanied by increased curvature especially at the lower energies, where absicca intercepts of 1.8 to 1.68 eV were observed.

It was shown that the photocurrent of these films possess an unusual voltage dependence, exhibiting in some cases two peaks. An attempt was made

to record the photocurrent's spectral response at voltages corresponding to or near the two maxima. It was observed that the two peaks shift by small amounts with time, the cathodic peak doing so more than the anodically positioned peak. The large dI/dV of the peaks' slopes and the shifting preclude making an accurate measurement of the spectral response, though qualitative observations can be made. The photocurrent spectrum of the films obtained at 0.3V to 0.5V were essentially the same as those obtained at 0.0V, the magnitude of the photocurrent was of course much greater. There was a difference observed at the more cathodic potentials (-0.4V to -0.15V), where, relative to the spectra measured at 0.0V, the photocurrent at the longer wavelengths, ~ 525 nm and above, were enhanced over the photocurrent at the shorter wavelengths.

The photocurrent spectral response of the thermal oxide films is shown in Figure 6. The same corrections applied to the r.f. oxide films were employed here. It can be seen that the same trend in the spectral shift with Ti content is evident. The enhanced photoactivity in the 425-600 nm region is quite obvious for the [4.4-5.3%] Ti samples, and as the Ti content is increased to [11.4%], the photoactivity curve returns approximately to the reference 0% curve. Unlike the r.f. oxides, the thermal oxides appear to have little or no photoactivity beyond 680 nm. The photocurrent's spectral response of the thermal oxide samples was also measured at potentials cathodic (-0.5V to -0.2V) and anodic (0.4V to 0.5V) of 0.0V and were equivalent to the spectral response obtained at 0.0V.

Using the same argument outlined above for the r.f. oxide where the photocurrent was assumed to be proportional to the absorption coefficient, the photocurrent vs wavelength data was replotted in the form $(I \cdot h\nu)^{1/2}$ vs $h\nu$. The approximately linear relationship observed suggests that the transition is

Relative photocurrent as a function of the excitation wavelength for the thermal oxide series of Fe/Ti oxide thin films. Each curve is normalized to 400 nm and has been corrected for variations in the excitation intensity. The solution is 1 M NaOH. The applied potential to each sample was 0.0 V (vs SCE).

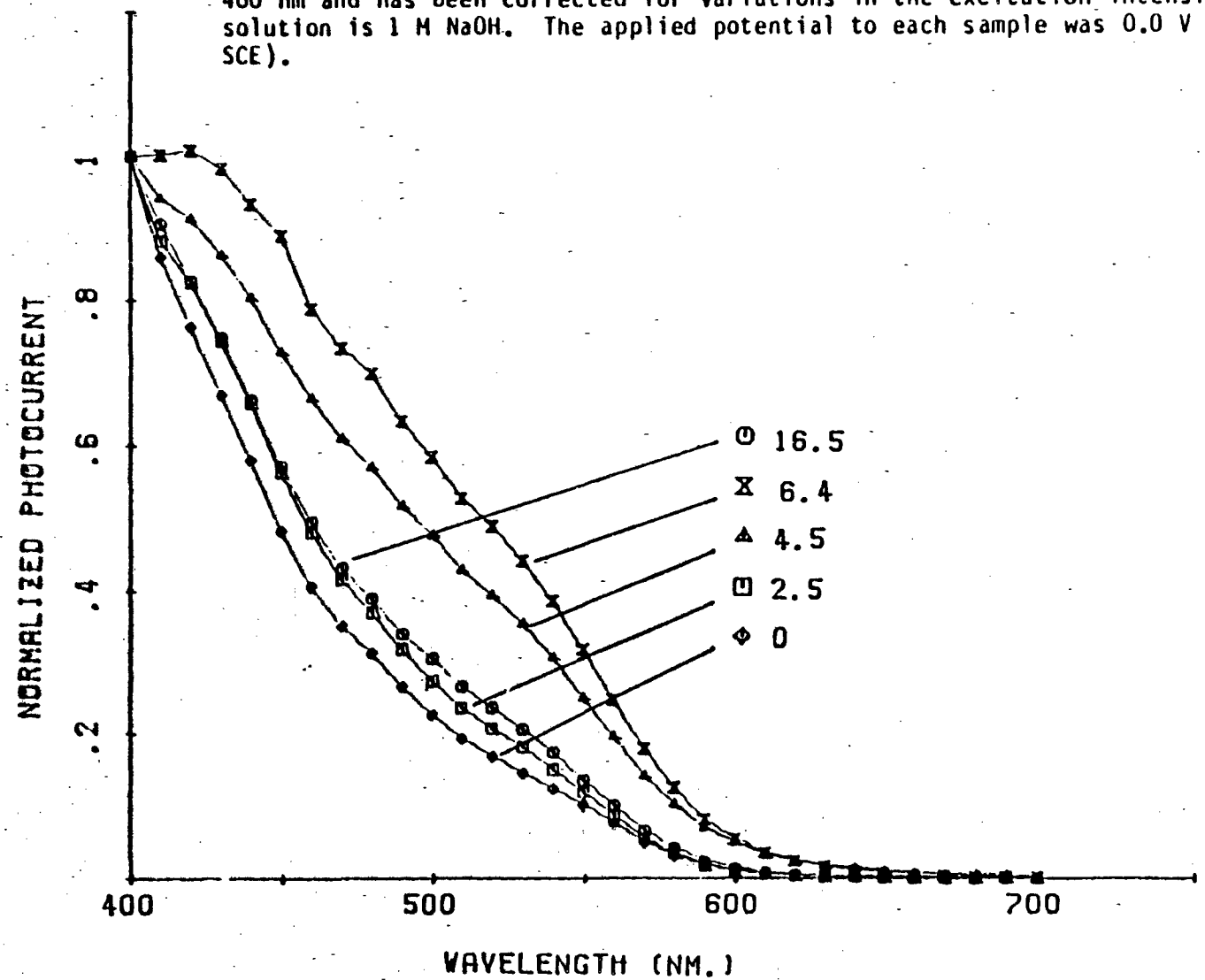

FIGURE 6

indirect. As with all the other plots of spectral data discussed so far, the thermal oxide spectral response also possessed some curvature in the low energy (<2.3 eV) regime. Unlike the r.f. oxide samples though, the reproducibility of this curvature from sample to sample was very good.

In many materials where band tailing is known to exist, due either to impurity effects on the valence and conduction bands, or to lattice deformation caused by impurities or structural irregularities, such as amorphicity, the absorption coefficient is often found to increase exponentially at the edge. This relationship described empirically by the equation[10]

$$\alpha = \alpha_0 \exp[\nu(h\nu - Eg)/kT]$$

is known as the Urbach rule.[11] The thermal oxide spectral response was plotted in the form ln (I) vs hν and it resulted in two linear segments, one from a low energy of 1.7 eV to 1.9 eV to an intermediate value of 2.2 eV to 2.3 eV and a second one with a much smaller slope extending to 3.25 eV.

A similar exercise was carried out with the spectral data obtained from the r.f. oxide films,. Although the overall form of the derived plots were the same as that obtained with the thermal oxide data, the obvious curvature in the plots was not at all convincing evidence that the Urbach type edge was present in the r.f. oxides.

Differential Capacitance

The differential capacitance of the r.f. oxide and thermal oxide films was usually measured at 23 Hz and a few films were measured at 500 Hz and 1

KHz; all were analyzed as a series resistor-capacitor network. The Mott-Schottky plots obtained from the capacitance data are somewhat complex, exhibiting regions of different slope. The curves were also double valued as can be seen in Figure 7. At the more anodic potentials, where the Mott-Schottky approximation[12,13] is no longer valid, the capacitance begins to increase as the semiconductor is being biased into the inversion region.

The flatband potentials (V_{FB}) were determined by the abscissa intercept of the curves and the results are shown in Table 3 and 4. The values listed are averaged over a number of measurements on the same sample and on different samples with nominally the same composition.

Table 3

R.f. Oxide Flatband Potential

Composition	Flatband Potential (1 M NaOH vs SCE)
0	-.61
[1.2]	-.63
[3.3]	-.65
[4.4]	-.56
[5.3]	-.4
[7.2]	-.37
[11.4]	-.43
[16.9]	+.87

Normalized (capacitance)$^{-2}$ verses voltage of a 1.2% Ti (Curve A) and a 11.4% Ti (Curve B) r.f. oxide film.

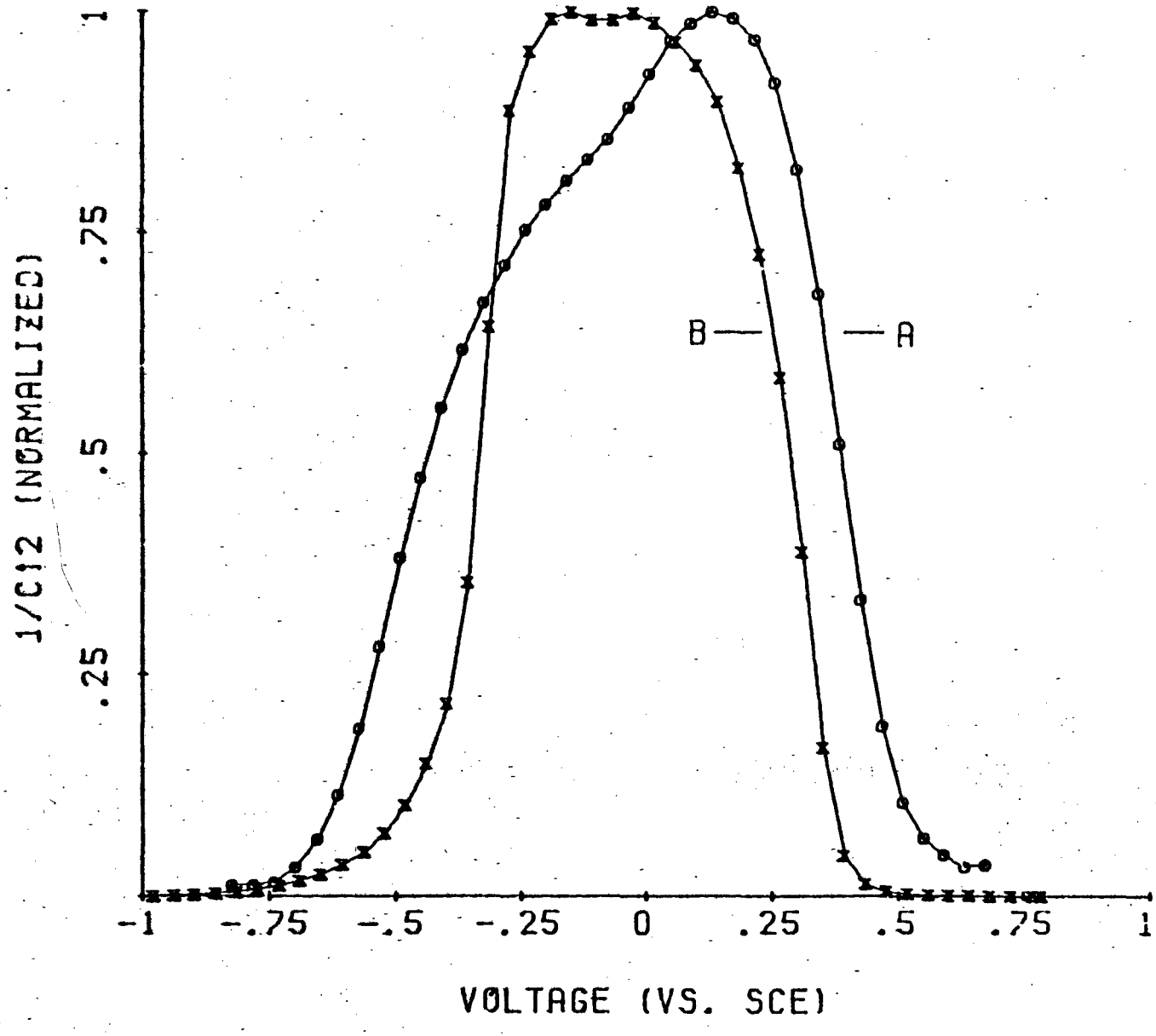

FIGURE 7

Table 4

Thermal Oxide Flatband Potential

Composition	Flatband Potential (1 M NaOH vs SCE)
0	-.74
[1.2]	-.77
[2.5]	-.75
[4.5]	-.77
[6.4]	-.79
[16.5]	-.70

The values for the r.f. oxides at low concentrations of Ti agree well with previously reported V_{FB}.[14,15,16] As the Ti content increases, the V_{FB} becomes more positive and at [11.4%] Ti it is -0.43V. When the Ti concentration is increased to [16.9%] Ti, the V_{FB} makes a large anodic jump to +0.87V. This positive V_{FB} reflects the fact that the material is now presumably p-type and the Fermi level is located near the valence band. It should be realized that the nature of the relationship between the space charge capacitance and applied voltage, which is double-valued, makes the V_{FB} determination equivocal, unless one knows beforehand the nature of the semiconductor being examined.

The V_{FB} obtained from the thermal oxide films, Table 4, behave differently than the r.f. oxide films in two aspects. First, the magnitude of the thermal oxide V_{FB} is more negative by 0.1 to 0.2 V than the corresponding low Ti content r.f. oxide sample. Secondly, unlike the r.f. oxide series, there isn't any positive shift in V_{FB} as the Ti content is increased; the V_{FB}

remains approximately constant throughout the upper Ti concentration range examined.

The charged impurity density (N_D) in the space charge region is also obtainable from the slope of the Mott-Schottky plot. More precisely, the product $N_D \cdot \varepsilon$ is determined, where ε is the material's dielectric constant. Values of ε are dependent not only on the intrinsic properties of a particular material but also on the macroscopic structure, particle size etc.; values of 10 to 120 have been used in the literature.[14,15,16] Because of this uncertainty we shall report the combined product $N_D \cdot \varepsilon$ and make the assumption that although ε is unknown, it is unlikely to be changing significantly.

At the low end of the Ti concentration range, the Mott-Schottky plots are qualitatively similar to that shown in Figure 7 curve A. There is an inflection point in the slope that occurs in the range of -0.35 V to -0.25 V, and is often not as well defined as that in Figure 7. At the higher Ti concentrations, this inflection point is not always obvious as it very often coincides with the onset of the plateau of the bell-shaped curve, Figure 7 curve B.

The value of $N_D \cdot \varepsilon$ varies from $10^{21} cm^{-3}$ to $10^{22} cm^{-3}$ in the low Ti regime, $0\% \leq \%\ Ti \leq 5.3\%$. At and beyond 5.3%, $N_D \cdot \varepsilon$ sharply decreases by an order of magnitude, $10^{20} cm^{-3}$ to $10^{21} cm^{-3}$. When the second linear segment anodic of the inflection point is apparent, the value of $N_D \cdot \varepsilon$ is 2 to 5 times the values obtained from the first linear segment. The Mott-Schottky plots obtained from the thermal oxide films were very similar from sample to sample, and resembled Figure 7 curve A. A representative curve is shown in Figure 8. The curves were linear from V_{FB} up to approximately -0.35 V to -0.30 V at which point there was a small inflection point. From this point, the curve again was

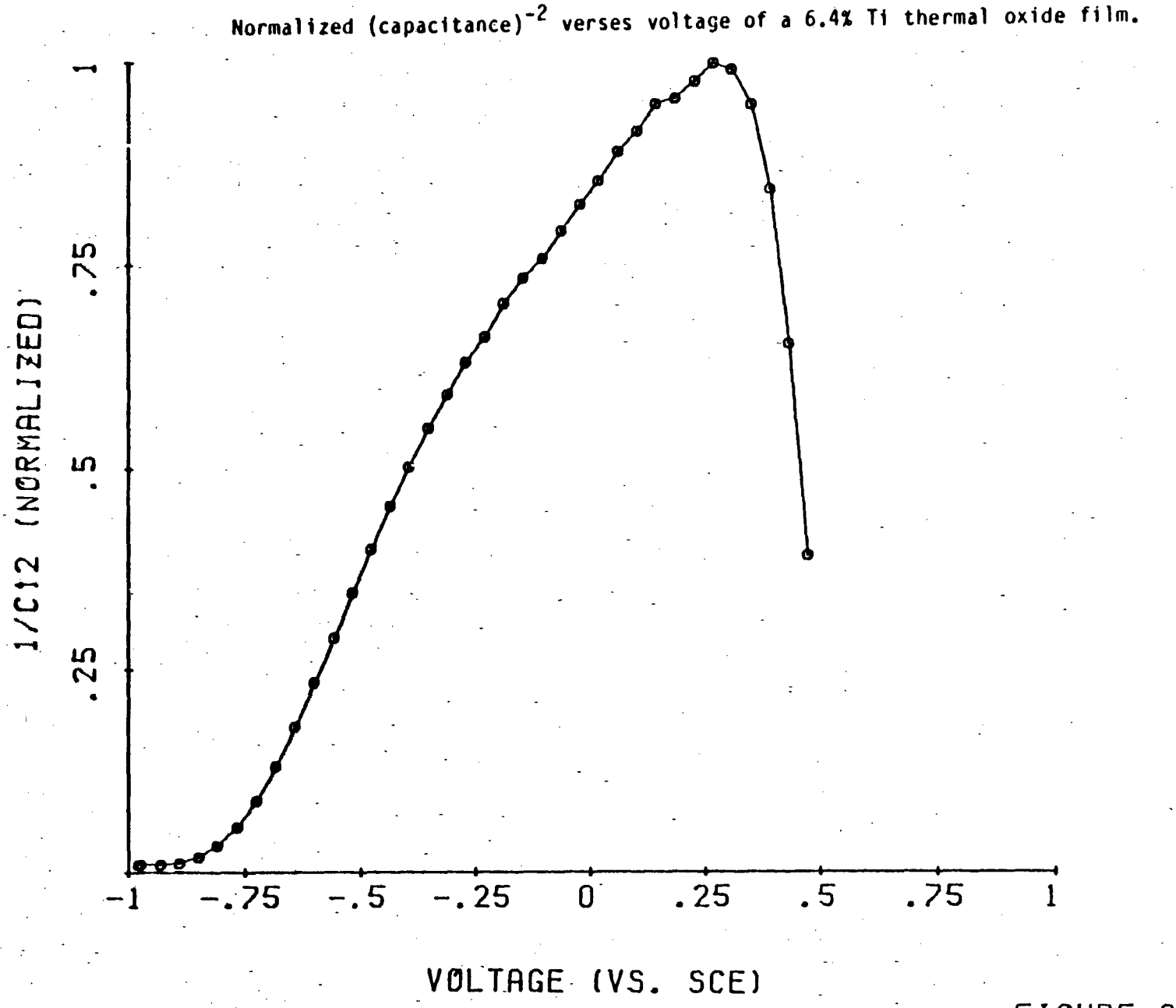
Normalized (capacitance)$^{-2}$ verses voltage of a 6.4% Ti thermal oxide film.
1/C12 (NORMALIZED)
1
.75
.5
.25
-1
-.75
-.5
-.25
0
.25
.5
.75
1
VOLTAGE (VS. SCE)

FIGURE 8

linear to approximately 0.5 V with a slightly diminished slope. The derived value of $N_D \cdot \varepsilon$ was relatively constant throughout the Ti containing thermal oxide films at $5 \times 10^{20} cm^{-3}$ to $3 \times 10^{21} cm^{-3}$. Anodic of the inflection point at approximately -0.35 V, the value of $N_D \cdot \varepsilon$ would usually increase by a factor of 2. The 0% Ti thermal film yielded an anomalously high value of 6×10^{23} for $N_D \cdot \varepsilon$.

Photoconversion Efficiency

The photoconversion efficiency (η) defined as electrons generated per incident photon, was determined for the r.f. oxides and thermal oxides. The efficiency was determined at 450 nm and an applied potential of 0.5 V. Within the r.f. oxide samples, the efficiencies varied from 0.1 to 1.3%, with most of the samples lying in the range of 0.4%. The conversion efficiency of the 0% sample was ~ 0.35%. The thermal oxides on the other hand had efficiencies which varied from 3-4% including the 0% Ti sample. There was one [16.5%] sample that exhibited a respectable 11% conversion efficiency.

Stability

Preliminary stability measurements have been made on a 0% and [5.3%] r.f. oxide. A small amount of dissolution was observed in the 0% Ti sample after 67 hours, but no decomposition was seen in the [5.3%] Ti sample after it was in solution for 96 hours and passed 13.9 coulombs of charge. The illumination source in both measurements was a 100 W Hg lamp.

Discussion

A discussion of the properties of these thin films, absorbance, photoconductivity and photoelectrochemistry, would normally be presented in terms of

comparisons with previously reported data on similar or related preparations. In this present system though, such an approach is not without some legitimate questions of appropriateness, because of the predominately amorphous character of these films. This non-crystalline character poses two problems dealing first with the composition, structural identity, and homogeneity of the films and secondly with validity of using a band model, derived for crystalline matter, as a framework to discuss the observed properties of these films. The amorphicity of these films, which implies the lack of long range structure, also precludes for the most part the determination of short-range structure as well.

This has consequences in terms of compositional ambiguities. In the present case, the Fe/Ti ratio was determined by the SIM technique, but SIMS is inexact when it comes to determining the amount of oxygen present. Often the identification of the crystal structure is sufficiently adequate to fix the relative ratio of metal ion to oxygen content, but this is not possible here. Consequently there are a number of questions that remain unanswered, such as what particular Fe oxide(s) are present, what are their spatial distributions, and how is the Ti incorporated in the film. Although these questions are unanswered, it is not unreasonable to speculate about what the film composition is and discuss it in terms of this composition as long as it is fully appreciated that it is indeed just speculation. Contained within the X-ray results is some evidence that may give more credence to our speculation. It was noted that in some of the r.f. oxides, without a underlying metal layer, a diffraction pattern consistent with the $Fe_2O_3/FeTiO_3$ structure could be extracted with a photographic averaging technique. The breath and weakness of these lines could result from a number of different conditions.

One possibility which would account for these results is that, contained within the bulk of a structurally ill-defined amorphous film, there is a very thin layer of polycrystalline material possibly subject to some lattice distortions due to internal stress. Another possibility, which is somewhat more appealing, is that essentially all of the r.f. oxide film is, in terms of the short-range order, considered to be of the $Fe_2O_3/FeTiO_3$ structure. The extent to which this short-range order is found could depend subtly on preparation conditions etc., such that in some of the films the short-range order may be extensive enough that hints of coherent diffraction are observed.

The situation with the thermal oxides is different than the r.f. oxides, as the oxide growth conditions are very much different. There has been a large body of work reported on the oxide growth on iron,[17-22] which indicate that nature of the oxide(s) is quite dependent on temperature and O_2 partial pressure, and under some circumstances, a glassy amorphous oxide layer has been observed. In all of the cases the low temperature films were of a stratified composition, with Fe_3O_4 at the interface between the film and crystalline metal surface, an intermediate γ-Fe_2O_3 layer and an outer α-Fe_2O_3 layer. To our knowledge, a similar study on the oxidation of an amorphous metal film has not been published. As to whether or not the thermal oxide films prepared in this study are similarly structured, it is of course not known. But the fact that the film, which forms when the underlying metal layer is completely consumed, is polycrystalline and only of the $Fe_2O_3/FeTiO_3$ structure argues against the presence of Fe_3O_4. It suggests that the bulk may be of one composition and structure, $Fe_2O_3/FeTiO_3$, as it is assumed to be in the r.f. oxide films.

The second area of difficulty presented by the amorphous nature of these films is the validity of using models derived from band theories to discuss

the properties of these films in terms of bandgap, well defined band edges, discrete impurity states in the gap etc. An essential element to all band structure construction and development is that the lattice is regular and orderly which allows for the coherent interaction of the various wavefunctions that make up the solid state bands. In an amorphous material where these orderly long-range interactions are not present, the conceptual basis of the band structure is in considerable doubt.

Amorphous semiconductors have been studied for many years, and it is interesting to note the many experimentally observed similarities with crystalline semiconductors. In many aspects the properties of amorphous semiconductor are adequately interpreted by a modified band structure which allows for a finite density of states in the gap, a band edge that is defined in terms of varying carrier mobility plus some other additional adjustments.[10,23] Unfortunately, little research has been directed at the electrochemistry and photoelectrochemistry of amorphous electrodes, presumably because conventional wisdom would indicate that the low mobilities and low efficiencies associated with amorphous semiconductors make them very unattractive materials for electrodes and unworthy of further consideration. Recently work[24] was published on a chemical vapor deposited $Fe_xTi_{1-x}O_y$ series of films ($0.0 \leq x \leq 0.9$) and it indicated the presence of amorphous films at a medium composition range ($0.1 \leq x \leq 0.7$). The amorphous films were shown to actually exhibit greater photocurrents than their annealed counterparts. Similar results were observed in the present study. Despite the problems that might be associated with discussing an amorphous solid within the framework of a band structure, the following sections will do so freely as comparisons are made between the present materials and results obtained from crystalline Fe_2O_3 and $FeTiO_3$.

Absorptivity

The absorptivity curve of the 0% Ti r.f. oxide is Figure 1 is very similar to other published spectra of Fe_2O_3, with respect to the onset of absorption (~ 2.0 eV), the small shoulder in the absorption band at ~ 500 nm and the absolute value of the absorptivity curve.[25-27] This correspondence supports the conclusions drawn from the X-ray results.

With small increases in the Ti concentration, the absorption in the 500 nm to 600 nm region increases and then the whole spectral curve decreases at the highest Ti concentrations. Little if any of these changes are due to a change in the bandgap, which except for some band tailing expected for amorphous or highly disorder materials, remains relatively fixed. The absorption changes are most likely due to variations in the density of states of the bands involved in the transition(s) and/or changes in the transition selection rules brought about by alterations of local molecular symmetries. Similar behavior has been seen in the diffuse reflectance spectra of polycrystalline $Fe_xTi_{1-x}O_3$[28], where it was shown that the addition of Ti^{+4}.Fe^{+2} results in donor levels which are located approximately 0.5 V to 0.6 V below the conduction band and empty d sublevels located approximately 0.2 eV above the conduction band (2.2 eV above the valence band).

It is not yet obvious why the absorptivity should decline with a continued increase in Ti beyond 5% as rapidly as it does. The bandgap of $FeTiO_3$ is reported to be 2.58 eV and as the concentration of Ti approaches 50%, the spectrum is expected to be blue-shifted. It is surprising to find the blue-shift occurring at such relatively low Ti concentrations (5.2 % $\leq$ % Ti < 16.9%), also without any apparent large shift in the bandgap.

The photoconductivity response is determined by both the absorption characteristics of a particular material and the spectral and spatial response

of the product term $\eta\mu\tau$, described earlier. If the term $\eta\mu\tau$ were constant, the photoconductivity curve would be identical to the absorption curve. The factors that come in to play in determining the various components of $\eta\mu\tau$ are quite complex and beyond the scope of this discussion. It can be argued that near the absorption edge there should be some similarity between the photoconductivity and optical absorption spectrum.[10] This is generally observed in amorphous semiconductors. At energies above the edge the photocurrents are relatively constant. Crystalline semiconductors, on the other hand, often exhibit a peak in the photoconductivity curve at photon energies just above the edge which is usually due to spatial variations in $\eta\mu\tau$. When the absorption coefficient is high, most of the light is absorbed in the outer regions of the material where surface effects tend to increase the recombination rate, thereby lowering the photocurrent.

From Figure 1, it would be expected that a similar spectral enhancement in the 450 nm to 600 nm region should be seen in the photoconductivity. It is seen in Figure 2 that initially there is a large increase in the response in going from 0% to 3.3% Ti, followed by a much more subtle change with a further increase in Ti. The 7.2% Ti photoconductivity curve, which defines the turnabout in the spectral enhancement like that seen in the absorptivity data at 5.3% Ti, does appear to be different from the rest of the Ti containing films. This particular film was the thinnest examined (540Å) and therefore the data was subject to the most manipulation in order to obtain the photoconductivity curve expected at a normalizing thickness of 760Å. Consequently its significance must be weighted accordingly.

The photoelectrolytic spectral characteristics should be quite similar to the photoconductivity curves since the photoelectrolysis currents also depend

on the absorptivity and a similar $n\mu\tau$ term. It can be seen in Figure 5 that the photoelectrolytic spectral profiles are not exactly equivalent to the photoconductivity curves, though the same enchanced response for Ti < 5.4% that is present in the other spectrally related data is also present here. The same decrease in photoactivity with Ti equal to 16.9% seen in the absorptivity data is also present. As in the absorptivity data, there is no unambiguous change in the bandgap aside from the postulated band tailing that suggests a decrease in the bandgap. It has been demonstrated in similar amorphous films[24] that as the Ti concentration increases from 30% to 75%, the photocurrents in the 600 nm to 450 nm continue to decrease without any shift in the bandgap. There is some question though as to exactly how similar these amorphous films are with respect to the present study, as they could see diffraction due to Fe_2TiO_5 and TiO_2 when the amorphous films were annealed in Ar at 600°C. This suggests the stoichiometry of their amorphous films may be different than the present amorphous films.

The voltage dependence of the photoelectrolytic current of these films contains two interesting and unusual features; the p-type photocathodic currents in the r.f. oxides and the existence of a distinct photoanodic current peak just positive of the V_{FB}. The photocathodic currents are normally observed at the highest Ti concentrations, 16.9%, though photocathodic currents were observed in the lower Ti containing samples when the sample was cathodically scanned the first time. After the cathodic scan was completed, the above mentioned peak would appear. Photocathodic currents are not uncommon in the literature of Fe_2O_3[16,29-30] and TiO_2 doped Fe_2O_3[24], though little effort has been made to explain behavior that is unusual for an n-type semiconductor. It has been suggested[16] that when the bias is cathodic of the

V_{FB}, the conduction band is bent downward and illumination increases the electron density near the surface giving rise to the observed photocurrents. At potentials where band bending is slight, this is certainly possible, but as the band is bent further, the electron density at the surface increases exponentially and the photogenerated electrons would contribute proportionately less to the overall cathodic current. Examination of the data in references 16 and 31 though indicate the photocathodic current is still increasing as the bias is made more negative.

In reference 16 the V_{FB} is defined as potential at which the n-type semiconductor's typical photoanodic current goes to zero and becomes a photocathodic current. In the context of the previously outlined explanation, this would be a reasonable determination of V_{FB}. Experimentally in Ref. 16 V_{FB} was found to be -0.22 V (vs SCE at pH 8.4) which is approximately 0.1 V positive of the V_{FB} as determined by the differential capacitance measurements. The reported examples of photocathodic currents were also positive of the V_{FB} as determined by the Mott-Shottky plot. In the present case, it is not felt that such an explanation is adequate because the photocathodic currents occur at potentials quite positive of V_{FB} (Mott-Shottky) and they are eliminated by a one time cathodic polarization of the electrodes. The cause of this particular phenomenon will have to wait for further study.

The photocathodic currents that are observed in the highest Ti containing films are, on the other hand, believed more likely due to the photoresponse of a true p-type semiconductor. The fact that $Fe_2O_3/FeTiO_3$ solid solutions are known[31] to switch from n-type to p-type at higher concentrations of $FeTiO_3$ gives us some confidence in our conjecture. Solid solutions of $Fe_2O_3/FeTiO_3$ in the form of sintered polycrystalline pellets were shown to have a Seebeck

voltage that changed continuously with composition. The sign of which was positive for Ti contents higher than 36.5%. This value is higher than what is presently observed, but the composition at which the change from n-type to p-type occurs will be dependent also on the different carrier mobilities. And it is not unreasonable to accept that these might be different in materials prepared by such vastly different techniques.

The other unusual aspect of the photocurrent's voltage dependence was the peak observed approximately 0.2 V to 0.3 V positive of the V_{FB}. This peak was predominate in the r.f. oxides (Ti < 16.9%) and to a lesser extent in the thermal oxides at the low end of the Ti concentration range. It was seen in the r.f. oxides (%Ti < 11.4%) that both the onset potential and the peak shifted anodically along with the V_{FB} as the Ti concentration increased. At higher Ti concentrations, the onset potential was not determinable because of the increasingly predominate photocathodic currents. The onset potential observed in the thermal oxide films similarly shifted positively with increasing Ti concentration even though the V_{FB} remained approximately constant. The peak in the thermal oxide films did not shift with the onset potential and was replaced by a low level plateau of photocurrent in the region of -0.55V to 0.0V. Anodic shifts[32] in the onset potential relative to V_{FB} with increased Ti doping have been observed before with the explanation that as donor density increases, the space charge region is narrowed and higher overvoltages are required to see measurable photocurrents.

It is unlikely that such is the case in the present thermal oxide films for two reasons. First, the differential capacitance data indicates the donor density does not change significantly as a function of Ti. Secondly the quantum efficiency at higher potentials (0.5V) are essentially independent of

Ti concentration indicating that the width of the space charge region is relatively constant. Another possibility, demonstrated[30] in certain preparations of Fe_2O_3, is the presence of surface states located a few tenths of an eV beneath the Fermi level. As long as the Fermi level is negative of these states, they can effectively quench the hole concentration via recombination processes. In the Ti containing films, a deep donor level which has been seen[14,28] before and whose existence is suggested in the present films by the differential capacitance data could similarly quench the hole concentration at the more cathodic potentials.

The presence of peaks in the photocurrent have been observed[16,33] at anodic potentials, coincident with the onset of substantial dark currents. These peaks have been attributed in one case[16] to an increased concentration of nonphotogenerated holes in the region of the space charge which effectively lowers the absorption coefficient. Another explanation[33] is that electron tunneling from the electrolyte or surface states to the conduction band results in some electrons recombining with the holes, thereby decreasing the photocurrent. These explanations may explain the frequently observed peaks seen in the present study at the higher anodic potentials where the dark current is increasing.

They do not, however, explain the peaks at potentials just positive of V_{FB}. We offer as a tentative explanation that these photocurrent peaks may be a consequence of Fermi level pinning by surface or interface states located approximately 0.6 V beneath the conduction band. These states may be associated with the deep donor states that are similarly located approximately 0.6 V beneath the conduction band. At this energy, these states are about 0.4 V negative of the O^2/OH^- redox couple in solution. As the bias on the

electrode is swept anodically, most of the varying potential is impressed across the Helmholtz layer because of the Fermi level pinning, resulting in a increased registration of the surface state energy with O_2/OH^- redox energy and a concomitant increase in photocurrent. Beyond some optimum potential, the increasing disparity between these same energy levels results in the decrease in photocurrent. This presumably is also accompanied by an "unpinning" of the Fermi level at the more anodic potentials. The applied voltage is now impressed predominately across the space charge region which grows according. The wider space charge region results in increased hole formation which leads to the usual increase in photocurrent at approximately 0.0 V.

The presence of such surface/interface states should have been observed[13] in the capacitance data as a region in which the capacitance changes very little with potential. It is also possible that the surface/interface states are not monoenergetic but rather have some relatively broad distribution. This situation could lead to the same photocurrent verses voltage dependence, but would be difficult to see in the differential capacitance data.

The differential capacitance data yielded reasonably linear Mott-Schottky plots that suggested the presence of a donor level approximately 0.3 V to 0.35 V beneath the Fermi level. Such donor levels have been observed[28] and are attributed to Fe^{+2} donor states, though some studies of Ti-doped Fe_2O_3[14] did not observe evidence of this level. The calculated donor densities ($N_D \cdot \varepsilon$) are somewhat high when compared to single crystal and polycrystalline data, but are comparable to values obtained from amorphous films.[24] In the r.f. oxide films, a sharp drop in $N_D \cdot \varepsilon$ was observed at 5.3% Ti, which corresponds roughly to the positive shift in V_{FB}. It is curious that despite the change in $N_D \cdot \varepsilon$

by approximately a factor of 10 that there was not any evidence that the quantum efficiency changed, as would be expected if the width of the space charge region is proportional to $(N_D \cdot \varepsilon)^{-1/2}$. The positive shift in V_{FB} with respect to Ti concentration has been observed[24] before for much larger concentrations of Ti, but the turnaround from n-type to p-type was not seen. The $N_D \cdot \varepsilon$ obtained for the thermal oxides are also quite high, but comparable to other amorphous films. It is also relatively constant with respect to the Ti concentration except for an anomaly at 0% which is not believed to be significant. It is interesting that the V_{FB} is considerably more negative than the r.f. oxides.

CONCLUSION

We have made thin films of Fe/Ti oxide by two different techniques which are believed to be solid solutions of Fe_2O_3 and $FeTiO_3$. An unusual feature of both series of films is that they are non-crystalline as determined by X-ray diffraction techniques. The addition of Ti ($FeTiO_3$) up to approximately 5% to 8% causes an increased spectral response, relative to Fe_2O_3, at photon energies above the bandgap. This enhancement was observed in the thin film absorptivity spectra, the photoconductivity spectra, and the wavelength dependence of the photoelectrolysis spectra. From the standpoint of solar driven photoelectrolytic applications, these observed modifications are in the direction of improved performance and applicability. Specifically, although the bandgap does not appear to change significantly, the enhanced absorbance and the resulting increase in photoactivity in the region immediately above the Fe_2O_3 bandgap, increases the collection effeciency of the solar flux in this important region. The effect is almost the same as if the bandgap has been lowered.

In the spectral measurements on the r.f. oxide films there is a suggestion that the bandgap may have been reduced, but the effects of excessive band tailing make the determination ambiguous. Higher concentrations of Ti result in a reduction of these spectral enhancements. The higher Ti concentrations in the r.f. oxides also result in a change in the semiconductor from n-type to p-type, which opens up some interesting possibilities in terms of a p-n tandem photoelectrolytic cell design. The Ti concentration dependence of the flat-band potential differed considerably for the two preparations. The V_{FB} in the thermal oxide films was essentially unaffected by the Ti concentration. The V_{FB} of r.f. oxide films on the other hand exhibited a very definite anodic shift with increasing Ti concentration.

There appears to be little effect on the photoelectrolytic quantum efficiency by the addition of Ti. Overall the thermal oxide films were about 6 to 10 times more efficient than the r.f. oxides. The efficiency of the thermal oxide films are approximately equivalent to what has been observed for a variety of polycrystalline and single crystal preparations. This in itself is very surprising as conventional wisdom would suggest that an amorphous semiconductor should be a very poor candidate for photoeletrolytic applications because of the low mobility and high recombination rates associated with the amorphous state.

The observation of a Ti concentration dependent spectral enhancement, p-type conduction and relatively high quantum efficiencies all indicate that this particular series of materials possess some very interesting chemistry and physics which are certainly worthwhile pursuing, in terms of basic science and practical applications. The amorphous structure of this films adds an additional aspect which requires further consideration and investigation. This is not only with respect to the present system alone but in more general

terms, the relationship between the structure and physics of amorphous semiconductors and their photoelectrochemical properties.

SINGLE CRYSTALS

Preparation

Single crystals of Fe_2O_3-$FeTiO_3$ have been grown by the flux-melt technique, using PbO and V_2O_5 as the flux medium. The constituents are placed in a Pt crucible and the crucible is brought up to 1300°C in an electrically heated vertical furnace. After 24 hours at 1300°C, the temperature is lowered by approximately 2C°/hr until the temperature reaches 850-900°C. The furnace is then turned off and allowed to cool to room temperature. The flux-encrusted crystals are then separated from the flux by boiling in HNO_3.

Elemental and Structural Analysis

The elemental stoichiometries of the single crystals were measured by a Kevex energy dispersion spectrometer (EDS). The relative amounts of Fe and Ti were determined from the integrated intensities of the K_α and K_β peaks at 4.51, 4.79, and 6.37, 6.58 eV, respectively. The surface of one single crystal was measured by the SIMS technique to provide a cross-check between the two techniques. EDS, rather than SIMS, was used to measure the composition of the single crystals because of the much greater ease of measurement afforded by EDS. The results are given in Table 5.

X-ray powder diffraction techniques were used to examine the structure of the $FeTiO_3$-Fe_2O_3 single crystals. Representative single crystals were taken from each batch and ground to a fine powder in a mortar and pestle. The powder was placed in 0.3 mm thin wall capillary tubing and placed in a Reed powder diffraction camera. Unlike the results seen with the thin films, the

diffraction photographs were sharp and well defined. The diffraction patterns were easily indexed to the rhombohedral space grouped of $Fe_2O_3/FeTiO_3$ and/or the orthorhombic space group of Fe_2TiO_5. The structures are indicated in Table 5.

In all of the crystals examined, a small amount of V and Pb were also seen. From the one sample examined by SIMS, the amounts were 0.5% V and 0.1% Pb.

Table 5

Starting Composition %Ti	Crystal Composition %Ti (EDS)		SIMS	Structure
0	0			Fe_2O_3
6.2				
8.7	5.2	Bulk		$Fe_2O_3/FeTiO_3$
	10.6	Surface	15	
9.3	3.6			$Fe_2O_3/FeTiO_3$
11.1				
17	4.2			Fe_2O_3/Fe_2TiO_5
23.5	32			Fe_2TiO_5

Experimental Procedure

Photoelectrolysis

The single crystals were attached to copper foil with conductive Ag paint. The entire surface of the copper foil, the copper wire attached to the

foil and all of the crystal except for an ~5 mm^2 area of the front face were potted in epoxy. The experimental setup is the same as that described in the thin film section.

Results

The photoelectrolytic spectra of the single $Fe_2O_3/FeTiO_3$ crystals examined were nearly identical to the response of Fe_2O_3. The current versus applied voltage were also quite similar, yielding an onset potential on the order of -0.5 V. Although the overall shape of the curves were similar, there were some differences observed in the magnitude of the photocurrents measured, which translate directly into quantum efficiency. Table 6 lists the composition and conversion efficiency of the samples examined.

Although the number of samples measured is not large enough to make a definitive statement, the hint of a trend is seen in Table 6. The higher conversion efficiencies are seen at the higher concentrations of Ti. Also it should be noted that the variation in conversion efficiencies within any one composition is quite small in comparison to that seen for the 0% samples (Fe_2O_3). This may be an indication that, according to one of our initial premises, the photoelectrochemical properties of "pure" Fe_2O_3 are strongly dependent upon preparation, and might be stabilized by the addition of Fe^{+2} via a structurally compatible material, i.e. $FeTiO_3$.

Table 6

Composition %Ti	Conversion Efficiency electron/photon
0.0	1.5
0.0	0.07
3.6	0.7
3.6	1.0
5.2	1.7
5.2	2.5
32.0 (Fe_2TiO_5)	0.0

DISCUSSION

We have examined a collection of Fe_2O_3 thin films made by two different techniques containing varying amounts of $FeTiO_3$. In these films, there is clearly a definite modification of the thin film's properties upon the addition of $FeTiO_3$. This can be seen in the consistent behavior of all the composition dependent measurements, spectral response of the photoconductivity, photocurrent versus applied potential, flatband measurements, absorbance and photoconductivity measurements. All of these measurements indicate the occurrence of dramatic changes in a narrow composition region ranging from approximately 2.5-14.4% ($FeTiO_3$).

From the standpoint of photoelectrolytic applications, these observed modifications are in the direction of improved performance and applicability. Specifically, although the bandgap does not appear to change significantly, the enhanced absorbance and the resulting increase in photoactivity in

the region immediately above the Fe_2O_3 bandgap, increases the collection efficiency of the solar flux in this important region. The effect is almost the same as if the bandgap has been lowered. Secondly, the movement of the flatband potential to more negative values further enhances the utility of this material in a practical photoelectrolytic application by reducing the necessity of applying an external bias. Also, the following point should be emphasized. It is well known that p-n photoelectrolytic systems are much better photoconversion devices because the combination of the two electrodes reduce the bandgap and flatband potential requirements of one another. In the current thin film systems, there is the possibility of p-type behavior at the high end of the $FeTiO_3$ composition range. The possibility of making p-n junctions simply by modifying the Ti concentration of a Fe-Ti oxide system has some very interesting and useful ramifications, which will be pursued.

The results obtained from the spectral response of the single crystals is quite disconcerting given the seemingly consistent picture developed with the thin films. The reason for such differences in behavior is not at all clear, as the single crystals and thin films are supposedly the same material. There is one possibiity though which was brought to light by the SIMS data, concerning the possible difference in the oxygen stoichiometry between the thin films and single crystals. It should be noted, before too much credence is placed on the significance of the numbers presented below, that the accuracy of SIMS in determining the oxygen concentration is very poor. The yield factor for oxygen is one of the lowest of all the elements. All of the thin film oxides that were examined had oxygen stoichiometries (formulated as metal O_x) of 1.13 ± 0.16. These values are much lower than that obtained from the single crystal, with a value 1.82 ± 0.2. It is possible then that the

results seen in the thin films is a combination effect of both oxygen vacancies and the presence of Fe^{+2} and Ti^{+4}. It will be interesting to see if similar spectral shifts can be induced in the single crystals by some reduction technique.

Finally, a point should be made regarding the conversion efficiencies seen for the various preparation techniques. Relative to the r.f. oxides, the thermal oxides have a conversion efficiency that is almost consistently a factor of ten larger. In comparison to the single crystals, the conversion efficiency of the thermal oxides is still approximately 1.5 to 2.0 times higher. There appears to be something special about these thermal oxide films in regard to conversion efficiency. It should also be remembered that there was one 33% $FeTiO_3$ film which had a conversion efficiency three times higher than the average. This is six times the single crystal results and 30 times that seen in the r.f. oxides.

REFERENCES

1. A. Fujishima and K. Honda, Nature 238, 37 (1972).

2. A number of recent reviews on the subject are available. For example, M. S. Wrighton, Chem. & Engn. News, Sept. 1979. A. J. Nozik, Ann. Rev. Phys. Chem. 29, 189 (1978). A. J. Bard, Science 207, 13 (1980).

3. H. Tributsch, Ber. Bun-Gesell. Physik. Chemie 81, 361 (1977); J Electrochem. Soc. 125, 1086 (1978).

4. T. E. Phillips, K. Moorjani, J. C. Murphy, and T. O. Poehler, J. Electrochem. Soc. 129, 1210 (1982).

5. P. Merchant, R. Collins, R. Kershaw, K. Dwight, and A. Wold, J. Solid State Chem. 27, 307 (1979).

6. B. Warner, P. Shive, J. Allen, C. Terry, J. Geomag. Geoelectr. 24, 353 (1972).

7. R. G. Burns, D. A. Nolet, K. M. Parkin, C. A. McCammon, and K. B. Schwartz in Mixed Valence Compounds, D. B. Brown, Ed. (Reidel, 1980), p. 295.

8. D. S. Ginley and M. A. Butler, J. Appl. Phys. 48, 2019 (1977).

9. E. J. Johnson in Semiconductors and Semimetals, Vol. 3, R. K. Willardson and A. C. Beer, Ed., Chap. 6, Academic Press, New York (1967).

10. N. F. Mott and E. A. Davis, Electronic Processes in Non-crystalline Materials, Clarendon Press, Oxford, (1971).

11. F. Urbach, Phys. Rev., 92, 1324 (1953).

12. J. F. Dewald, J. Phys. Chem. Solids, 14, 155 (1960) and J. F. Dewald, Bell Syst. Tech. J., 39, 615 (1960).

13. S. R. Morrison, Electrochemistry at Semiconductor and Oxidized Metal Electrodes, Chap. 4 and 5 and references therein, Plenum Press, New York (1980).

14. J. H. Kennedy and K. W. Frese, Jr., J. Electrochem. Soc. 125, 723 (1978).

15. R. K. Quinn, R. D. Nasby and R. J. Baughman, Mater. Res. Bull., 11, 1011 (1976).

16. S. W. Wilhelm, K. S. Yun, L. W. Ballenger, and N. Hackerman, J. Electrochem. Soc., 126, 419 (1979).

17. N. Ramasubramanian, P. B. Sewel, and M. Cohen, J. Electrochem. Soc., 115, 12 (1968).

18. R. Francis and D. G. Lees, Corros. Sci., 16, 867 (1976).

19. D. Caplan and M. Cohen, Corros. Sci., 6, 321 (1966).

20. R. J. Hussey, G. I. Sproule, D. Caplan, and M. J. Graham, Oxid. Met., 2, 65 (1977).

21. A. G. Goursat and W. Smeltzer, Oxid. Met., 6, 101 (1973).

22. R. R. Ruf and R. J. Gambino, J. Appl. Phys., 55, 2628, (1984).

23. M. H. Cohen, H. Fritzsche, and O. R. Ovshinsky, Phys. Rev. Lett., 22, 1065 (1969).

24. B. Danzfuss and U. Stimming, J. Electroanal. Chem., 164, 89 (1984).

25. R. F. G. Gardner, F. Sweett, and D. W. Tanner, J. Phys. Chem. Solids, 24, 1183 (1963).

26. D. C. Lewis and W. D. Westwood, Canadian Journal of Physics, 42, 2367 (1964).

27. S. P. Tandon and J. P. Gupta, Spectroscopy Letters, 3 (11&12), 297 (1970).

28. S. V. Kosheheev and A. E. Cherkashin, Izvestiya Akademii Nauk SSSR, Neorganicheskie Materialy, 19, 1875 (1983).

29. P. Iwanski, J. S. Curran, W. Gissler, and R. Memming, J. Electrochem. Soc., 128, 2128 (1981).

30. M. P. Dare-Edwards, J. B. Goodenough, A. Hamnett, and P. R. Trevellick, J. Chem. Soc. Faraday Trans., 79, 2027 (1983).

31. Y. Ishikawa, J. Phys. Soc. Japan 13, 37 (1958).

32. J. H. Kennedy and K. W. Frese, Jr., J. Electrochem. Soc., 135, 723 (1978).

33. H. Ono, H. Morisaki, and K. Yazawa, Jpn. J. Appl. Phys., 21, 1075 (1982).

PUBLICATIONS

1. T. E. Phillips, K. Moorjani, J. C. Murphy, and T. O. Poehler, "TiO_2-VO_2 Alloys--Reduced Bandgap Effects in the Photoelectrolysis of Water," Bull. Am. Phys. Soc. 26, 283 (1981).

2. T. E. Phillips, K. Moorjani, J. C. Murphy, and T. O. Poehler, "TiO_2-VO_2 Alloys -- Reduced Bandgap Effects in the Photoelectrolysis of Water," Proceedings of Symp. on Photoelectrochem. Processes and Measurement Tech. for Photoelectrochem. Solar Cells 82-3, 673 (1982).

3. T. E. Phillips, K. Moorjani, J. C. Murphy, and T. O. Poehler, $Ti_{1-x}V_xO_2$ Alloys - Reduced Bandgap Effects in Photoelectrolysis of Water," J. Electrochem. Soc. 129, 1210 (1982).

4. T. E. Phillips, K. Moorjani, J. C. Murphy, and T. O. Poehler, "The Photoconductive and Photoelectrolytic Properties of Iron-Titanium Oxide Thin Films, " Bull. Am. Phys. Soc. 30, 441 (1985).

5. T. E. Phillips, K. Moorjani, J. C. Murphy, and T. O. Poehler, "Photoelectrochemical Properties of Iron-Titanium Oxide Thin Films," to be submitted to the Journal of the Electrochemical Society.

PRESENTATIONS

American Physical Society, Phoenix, March 1981, TiO_2-VO_2 Alloys -- Reduced Bandgap Effects in the Photoelectrolysis of Water, T. E. Phillips, K. Moorjani, J. C. Murphy and T. O. Poehler.

The Electrochemical Society Meeting, Denver, October 1981, TiO_2-VO_2 Alloys -- Reduced Bandgap Effects in the Photoelectrolysis of Water, T. E. Phillips, K. Moorjani, J. C. Murphy and T. O. Poehler.

American Chemical Society Meeting, Washington, D.C., August 1983, Photoelectrochemical Properties of Iron-Titanium Oxide Films, T. E. Phillips, K. Moorjani, J. C. Murphy, and T. O. Poehler

American Physical Society, Baltimore, March 1985, Photoconductive and Photoelectrochemical Properties of Iron-Titanium Oxide Thin Films, T. E. Phillips, K. Moorjani, J. C. Murphy, and T. O. Poehler.

END

FILMED

7-85

DTIC